STOCHASTIC FINITE ELEMENT THERMAL ANALYSIS OF A BALL GRID ARRAY PACKAGE

by

RAHUL UPRETI

Presented to the Faculty of the Graduate School of

The University of Texas at Arlington in Partial Fulfillment

of the Requirements

for the Degree of

MASTER OF SCIENCE IN MECHANICAL ENGINEERING

THE UNIVERSITY OF TEXAS AT ARLINGTON

MAY 2018

Acknowledgments

First and foremost, I would like to thank Dr. Dennis for his guidance and constant support throughout my research. His brilliant way of explaining concepts and tackling problems has taught me a lot.

Second, I would like to thank Dr. Han and Dr. Wang for serving in my master's defense committee.

I would also like to thank my parents and my aunt Janki Joshi, for their unconditional support towards my higher education. They have sacrificed a lot for me to receive higher education. I can never repay that.

I am also thankful to Kanishka Tyagi for being my mentor and giving me right advice whenever I needed it.

I would also like to thank Siddarth, Ashkan, James, and Sandeep for helping me with this work.

Lastly, I would like to thank my friends Deevika, Anubhav, and Dilraj for their constant support and motivation throughout my research.

April 19th, 2018

Abstract

STOCHASTIC FINITE ELEMENT THERMAL ANALYSIS OF

A BALL GRID ARRAY PACKAGE

RAHUL UPRETI, MS

The University of Texas at Arlington, 2018

Supervising Professor: Brian Dennis

This study provides an insight into the factors which have a major impact on the probability of failure of a Ball Grid Array package. A stochastic finite element analysis was done on the package using First-order reliability method (FORM). The effects of uncertainty in material thermal conductivities, heat source, heat transfer coefficient and ambient temperature were studied. The average temperature at the die-junction interface was selected as failure criterion because the excess temperature at the junction is often a cause of failure.

The performance of Finite Difference Method(FDM) and Semi-Analytic Complex Variable Method(SACVM) in computing sensitivities are compared. Results show that for some parameters, the probability of failure is more sensitive to uncertainties than other parameters, which provides crucial information to select the manufacturing tolerance of material properties and tolerance for parameters which are controlled experimentally. For sensitive parameters, a tighter manufacturing tolerance will decrease the randomness and ultimately increase the

reliability. The parameters for which probability of failure show low sensitivity with respect to uncertainties, large tolerance for manufacturing could be selected which will drop down the cost.

CONTENTS

List of Illustrations

List of Tables

Chapter 1 INTRODUCTION

According to Moore's law, computing speed doubles every two years. The increase in the speed of these chip, however, has slowed down during recent years. The main cause of this slowdown is the need for rigorous heat management to keep the chip from excessive failure temperatures. Efficient design and cooling solutions have become the most crucial factors in modern day chip design. The thermal conductivities of materials, cooling speed of fans, atmospheric temperature, and heat produced by the die, all have a significant role in determining the performance and reliability of the chip. In this study, we analyze the effects of uncertainties present in these properties on the probability of failure of a Ball Grid Array(BGA) package.

Almost every parameter in engineering systems has a certain degree of uncertainty. These uncertainties in parameters may result in outcomes which are misleading or unforeseen. The deterministic finite element approach, which is a norm in the industry, is incapable of incorporating the effects of uncertainty on the end results. Stochastic Finite Element Analysis is a tool which can use this uncertainty in data to make designs safer and more reliable. Stochastic Finite Element Method(SFEM) extends the conventional Finite Element Method to include problems which have randomness associated with input variables, making it a very powerful tool to produce highly reliable results. The gain in popularity of SFEM lately is because of the availability of abundant computational resources [4].

The probabilistic approach of SFEM, in which probability of failure is evaluated to determine the safety of the system, is widely used in marine industry. This calculation often involves a multidimensional integration of non-linear functions, which makes it very difficult to evaluate. First order reliability method (FORM) is used to linearize the performance function (also called limit state function), which determines the failure criterion for the system. Hasofer and Lind [18] developed Advanced First Order Second Moment method (AFOSM), which was applicable only for Gaussian distribution. Rackwitz et al. [9] discussed methods to use AFOSM for non-gaussian distributions. Over the years AFOSM evolved into what is currently known as FORM [1]. FORM has been widely used by researchers to determine the reliability of structures. Yanfang et al. [19] showed that FORM calculates the probability of failure and sensitivities of the probability of failure with low errors for both linear and non-linear limit state functions when compared to Monte-Carlo method. Parameswaran et al. [20] used FORM to evaluate the probability of failure of a one-dimensional heat transfer problem. They compared FORM with Monte-Carlo method and showed that FORM computes accurate results in few steps as compared to Monte-Carlo which required 100000 runs to compute the probability of failure. They also presented that FORM calculates the probability of failure accurately when the probability of failure was very low, whereas, Monte-Carlo could not compute it accurately even though it took an enormous number of samples and processing time. Jin et al. [21] used Semi-

Analytic Complex Variable Method (SACVM) to compute accurate sensitivities in reliability analysis of a 2-D heat transfer problem using FORM. Abubakar et al. [22] used FORM and Monte-Carlo method to evaluate the reliability of a counter flow heat exchanger and observed great agreement in the values of reliability index obtained by both the methods. They showed that net gain from the operation of heat exchanger calculated by deterministic approach had only 8.4% probability of occurrence, which demonstrated the need for stochastic performance analysis. Hirohata et al. [23] used FORM to perform multidisciplinary reliability analysis of CPU module packaging. Although there are only a few papers available in the literature which used FORM for heat transfer problems, the ones which are available show agreement in that FORM is computationally efficient than Monte-Carlo method and produce reasonably accurate results when compared to Monte-Carlo method.

Because of its computational efficiency, we used FORM to analyze the probability of failure of a Ball Grid Array Package and study how the uncertainty in input parameters affect the probability of failure. This analysis requires defining a performance function (or limit state function) which defines the failure criterion for the BGA package. We defined the limit state function as the average temperature at the silicon die and heat spreader interface, $g = T_{avg} - 97$, where T_{avg} is the average temperature at the interface of die and heat-spreader. T_{avg} depends on a lot of factors such as thermal conductivities of materials, heat transfer

coefficient, ambient temperature, etc. The uncertainties in these parameters could affect the reliability of design. We studied the effect of uncertainties present in these parameters on the probability of failure of the package.

Chapter 2 is a discussion of the underlying theory used in this study. Section 2.1 discusses the Finite Element Method and its application in solving the governing equation. Section 2.2 discusses the Stochastic Finite Element Method, which incorporates the uncertainties present in the parameters to calculate the probability of failure of the system. Section 2.3 contains the details of sensitivities calculation using FDM and SACVM.

Chapter 3 presents the details of the steps and methods used in this study. All the results are presented in chapter 4 in details. Chapter 5 presents the conclusion and future work.

Chapter 2 THEORY

2.1. Finite Element Method

Finite element method(FEM) is a very powerful tool used in the engineering industry for solving complex problems. The basic idea behind FEM is to divide the geometry into finite elements and generate a system of algebraic equations which can be solved to get the solution at nodes and generate a global function for the solution.

2.1.1 Galerkin's Finite Element Method

This method is based on Galerkin's method in which a strong form of the differential equation is transformed into a weak form and the solution is obtained using weighted-residual approach. In FEM, however, the domain is divided into finite elements instead of considering the whole geometry as one element. The steps in a finite element method analysis are shown in the flowchart below.

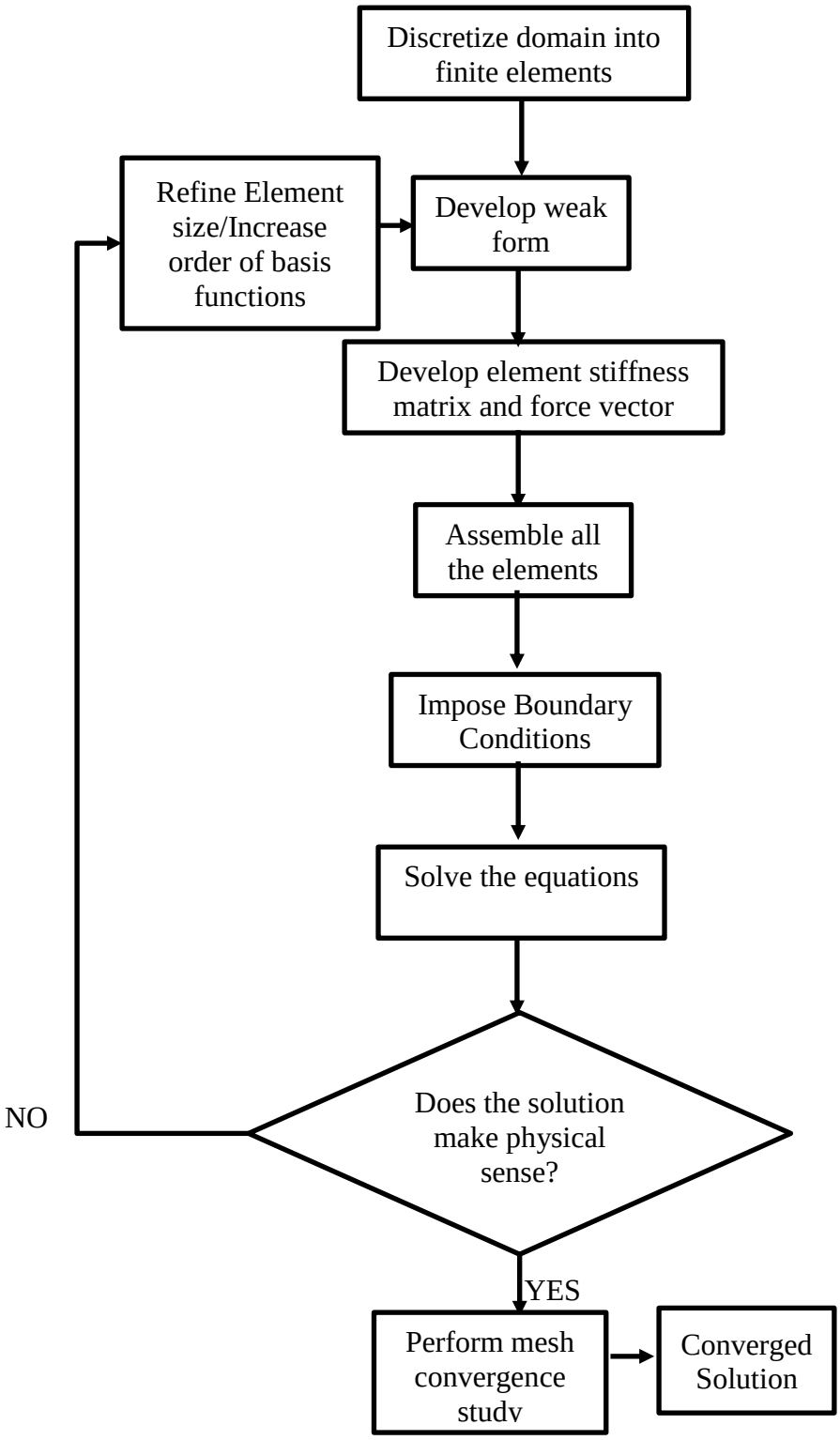

Figure 2.1 Flowchart of Finite Element Method

For steady-state heat transfer problems, the governing equation is

$$\frac{\partial}{\partial x}\left(k_x \frac{\partial T}{\partial x}\right) + \frac{\partial}{\partial y}\left(k_y \frac{\partial T}{\partial y}\right) + \frac{\partial}{\partial z}\left(k_z \frac{\partial T}{\partial z}\right) + Q = 0 \qquad (2.1)$$

where k_x, k_y, and k_z are the thermal conductivities in the x, y, and z directions respectively and Q is the heat generation per unit volume. To solve this problem using FEM, first we need to divide the domain into finite elements and then T is approximated over each element using a set of basis functions.

$$T^e(x, y) = \sum_{i=1}^{N} T_i^e \psi_i^e \qquad (2.2)$$

where T_i^e represents the value of temperature at nodal points of the element and ψ_i^e represents the basis function associated with the element and $T^e(x, y)$ is the temperature at any (x, y) location inside the element. These nodal temperatures must weakly satisfy the governing equation and boundary condition, meaning that the solution only need to satisfy C_1 continuity at the nodes even though the governing equation is second order. The transformation of strong form to weak form, which is basically integration by-parts, reduces the C2 continuity requirement of T to C1 continuity.

2.1.1.1 Weak form

The weighted-residual statement of equation (1.1) is given by

$$\int_{\Omega^e} w\left(\frac{\partial}{\partial x}\left(k_x \frac{\partial T}{\partial x}\right) + \frac{\partial}{\partial y}\left(k_y \frac{\partial T}{\partial y}\right) + \frac{\partial}{\partial z}\left(k_z \frac{\partial T}{\partial z}\right) + Q\right) d\Omega = 0 \qquad (2.3)$$

The above expression represents the residual of error when we substitute T_i into the differential equation, where w is the weight function and Ω^e represents the domain of element e. Since the governing equation is second order, T_i should be C_2 continuous. However, if we use integration-by-parts on equation (2.3), this requirement is weakened to C_1 continuity as shown in the equation (2.4), assuming k_x, k_y, and k_z are invariant with respect to space.

$$\int_{\Omega^e}\left(k_x\frac{\partial w}{\partial x}\frac{\partial T}{\partial x}+k_y\frac{\partial w}{\partial y}\frac{\partial T}{\partial y}+k_z\frac{\partial w}{\partial z}\frac{\partial T}{\partial z}-wQ\right)d\Omega - \oint_{\Gamma^e} w\left(k_x\frac{\partial T}{\partial x}n_x+k_y\frac{\partial T}{\partial y}n_y+k_z\frac{\partial T}{\partial z}n_z\right)d\Gamma=0 \tag{2.4}$$

If we consider a general formulation including conductive heat flux as well convective heat flux at the boundary equation 2.4 can be written as following [13].

$$\int_{\Omega^e}\left(k_x\frac{\partial w}{\partial x}\frac{\partial T}{\partial x}+k_y\frac{\partial w}{\partial y}\frac{\partial T}{\partial y}+k_z\frac{\partial w}{\partial z}\frac{\partial T}{\partial z}-wQ\right)d\Omega - \oint_{\Gamma^e} w(q_n-h(T-T_\infty))d\Gamma=0 \tag{2.5}$$

where q_n is the contribution of conductive heat flux, $h(T-T_\infty)$ is the contribution of convective heat flux, h is the heat transfer coefficient, and T_∞ is the ambient temperature. This formulation is called the weak statement. Here Ω represents the domain and Γ represents the boundary of that domain. In Galerkin's FEM, weight functions are also approximated using the same basis functions as T.

$$w^e(x,y) = \sum_{i=1}^{N} v_i \psi_i^e \tag{2.6}$$

The basis functions must be linearly independent and must satisfy the requirement of C_1 continuity.

2.1.2 Library of Finite Elements

2.1.2.1 Triangular Elements

The most common triangular element contains three nodes at its vertices. The basis functions are given by the following expressions

$$\Psi_1 = \frac{1}{2A}[(x_2y_3 - x_3y_2) + (y_2 - y_3)x + (x_3 - x_2)y] \tag{2.7}$$

$$\Psi_2 = \frac{1}{2A}[(x_3y_1 - x_1y_3) + (y_3 - y_1)x + (x_1 - x_3)y] \tag{2.8}$$

$$\Psi_3 = \frac{1}{2A}[(x_1y_2 - x_2y_1) + (y_1 - y_2)x + (x_2 - x_1)y] \tag{2.9}$$

where A is the area of the triangular element and (x_1, y_1), (x_2, y_2), and (x_3, y_3) are the coordinates of the vertices.

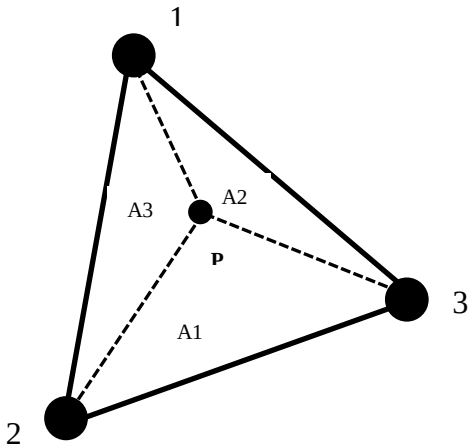

Figure 2.2 Triangular Element

These basis functions can also be expressed in area coordinates as

$$L_1 = \frac{A_1}{A} \tag{2.10}$$

$$L_2 = \frac{A_2}{A} \tag{2.11}$$

$$L3 = \frac{A_3}{A} \tag{2.12}$$

where A1, A2, and A3 are the areas formed by nodes P-2-3, P-1-3, and P-1-2 respectively. Here, P (x, y) represents any general point inside the triangle 123. L_i has a value of 1 at the i^{th} node and a value of 0 at every other node. The sum of L_1, L_2, and L_3 always adds up to 1. The field variable inside the element is expressed as

$$u(x, y) = u_1 L_1 + u_2 L_2 + u_3 L_3 \tag{2.13}$$

where u_1, u_2, and u_3 are the values at the nodes 1, 2, and 3 respectively.

2.1.2.2 Rectangular Element

The simplest kind of rectangular element has 4 nodes located at the vertices of the rectangle.

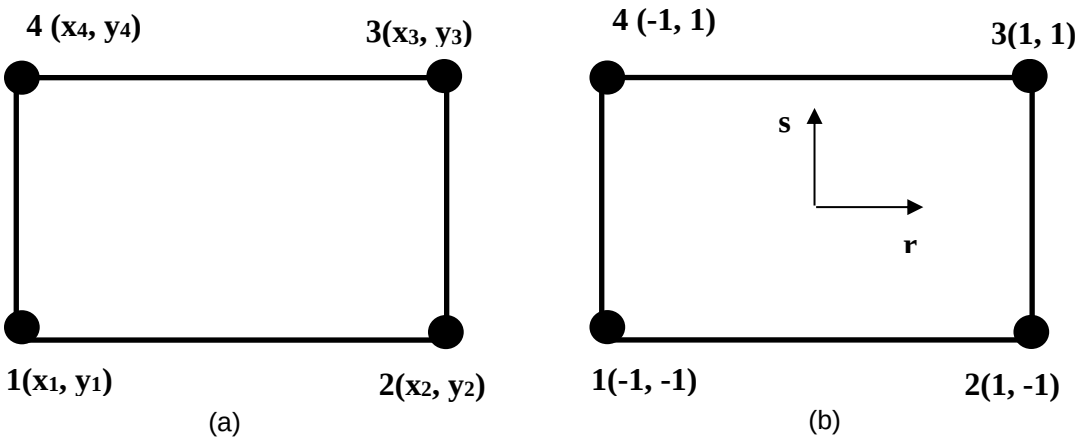

Figure 2.3 Linear Rectangular Element (a) in original coordinate system (b) in reduced coordinate system

The rectangle in the global coordinates is reduced to normal coordinates (r, s) as

$$r = \frac{x - \overline{x}}{a} \tag{2.14}$$

$$s = \frac{y - \overline{y}}{b} \tag{2.15}$$

Where $(\overline{x}, \overline{y})$ is the centroid of the rectangle in the global coordinates and a and b are the length and width of the rectangle respectively. The basis functions are:

$$\Psi_1(r,s) = \frac{1}{4}(1-r)(1-s) \tag{2.16}$$

$$\Psi_2(r,s) = \frac{1}{4}(1+r)(1-s) \tag{2.17}$$

$$\Psi_3(r,s) = \frac{1}{4}(1+r)(1+s) \tag{2.18}$$

$$\Psi_4(r,s) = \frac{1}{4}(1-r)(1+s) \tag{2.19}$$

Ψ_i has a value of 1 at the i^{th} node and value of zero at every other node. Basis functions for rectangle element with eight nodes can be defined in a similar manner.

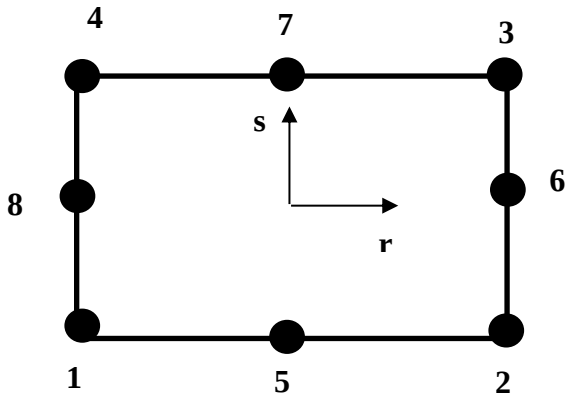

Figure 2.4 Second Order Rectangular Element

$$\Psi_1(r,s) = \frac{1}{4}(r-1)(1-s)(r+s+1) \tag{2.20}$$

$$\Psi_2(r,s) = \frac{1}{4}(r+1)(1-s)(s-r+1) \tag{2.21}$$

$$\Psi_3(r,s) = \frac{1}{4}(r+1)(1+s)(s+r+1) \tag{2.22}$$

$$\Psi_4(r,s) = \frac{1}{4}(r-1)(1+s)(r-s+1) \tag{2.23}$$

$$\Psi_5(r,s) = \frac{1}{4}(1-r^2)(1-s) \tag{2.24}$$

$$\Psi_6(r,s) = \frac{1}{4}(1-s^2)(1+r) \tag{2.25}$$

$$\Psi_7(r,s) = \frac{1}{4}(1-r^2)(1+s) \tag{2.26}$$

$$\Psi_8(r,s) = \frac{1}{4}(1-s^2)(1-r) \tag{2.27}$$

The field variable anywhere inside the element is represented by the following expression, in which N is the number of nodes in the element and u_i is the value at the i^{th} node.

$$u(x,y) = \sum_{i=1}^{N} u_i \Psi_i \tag{2.28}$$

2.1.2.3 Tetrahedral Elements

Just like the concept of area coordinates in the triangular element, a concept of volume coordinates can be used to represent the basis functions for a 4-node tetrahedral element. The figure below depicts a 4-node tetrahedral with a general point P inside it.

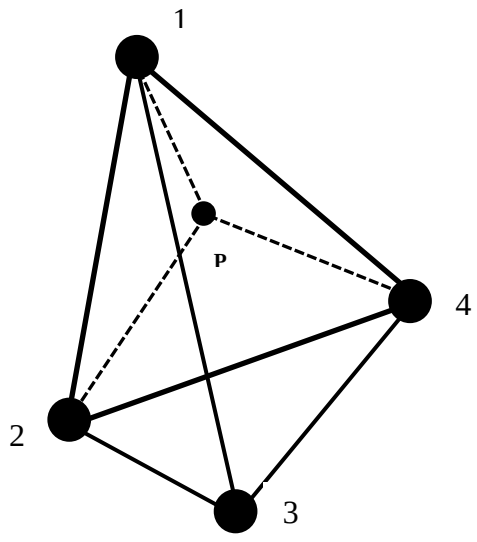

Figure 2.5 Tetrahedral Element

The volume coordinates are defined as

$$L_1 = \frac{V_1}{V} \tag{2.29}$$

$$L_2 = \frac{V_2}{V} \tag{2.30}$$

$$L_3 = \frac{V_3}{V} \tag{2.31}$$

$$L_4 = \frac{V_4}{V} \tag{2.32}$$

where V_1=Vol(P234), V_2=Vol(P134), V_3=Vol(P124), V_4=Vol(P123), and V is the volume of the tetrahedral 1234. The field variables are then represented by the following expression.

$$u = L_1u_1 + L_2u_2 + L_3u_3 + L_4u_4 \tag{2.33}$$

where u_1, u_2, u_3, and u_4 are the values at the nodes 1, 2, 3, and 4 respectively.

2.1.2.4 Hexahedral Elements (Brick Elements)

The idea of a two-dimensional rectangular element can be extended to three-dimensional brick elements. The brick element in reduced coordinate is shown in figure 2.6. The reduced coordinates are defined as

$$r = \frac{x - \overline{x}}{a} \tag{2.34}$$

$$s = \frac{y - \overline{y}}{b} \tag{2.35}$$

$$t = \frac{z - \overline{z}}{c} \tag{2.36}$$

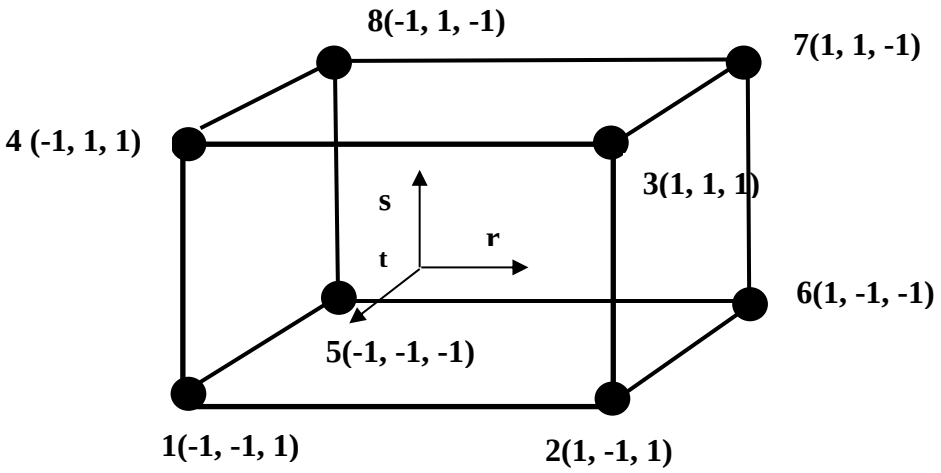

Figure 2.6 Hexahedral Element

The domain of the element in reduced coordinates is -1 to +1 in every direction. The basis functions are expressed as

$$\Psi_1 = \frac{1}{8}(1-r)(1-s)(1+t) \tag{2.37}$$

$$\Psi_2 = \frac{1}{8}(1+r)(1-s)(1+t) \tag{2.38}$$

$$\Psi_3 = \frac{1}{8}(1+r)(1+s)(1+t) \tag{2.39}$$

$$\Psi_4 = \frac{1}{8}(1-r)(1+s)(1+t) \tag{2.40}$$

$$\Psi_5 = \frac{1}{8}(1-r)(1-s)(1-t) \tag{2.41}$$

$$\Psi_6 = \frac{1}{8}(1+r)(1-s)(1-t) \tag{2.42}$$

$$\Psi_7 = \frac{1}{8}(1+r)(1+s)(1-t) \tag{2.43}$$

$$\Psi_8 = \frac{1}{8}(1-r)(1+s)(1-t) \tag{2.44}$$

Each basis function has a value of 1 at its node and value of 0 at every other node. The field variable is finally expressed as

$$u(x,y,z) = \sum_{i=1}^{8} \Psi_i u_i \tag{2.45}$$

where u_i is the value at the i^{th} node.

2.1.3 Coordinate Transformation

Although the elements discussed in previous sections can span the domain for simple geometries, they are not so useful for complex geometries with curved edges. To overcome this shortcoming, geometry is usually meshed with elements that have curved edges which are then transformed to the simple known elements through coordinate transformation. This transformation does not actually change the elements or the domain, but it is only done to evaluate the integrals in the weak form as those integrals are easy to evaluate for elements discussed in section 2.1.2. The transformation between the actual element and the equivalent master element is represented by the following expression

$$x = \sum_{i=1}^{n} \Psi_i(r,s,t) x_i \tag{2.46}$$

$$y = \sum_{i=1}^{n} \Psi_i(r,s,t) y_i \tag{2.47}$$

$$z = \sum_{i=1}^{n} \Psi_i(r,s,t) z_i \tag{2.48}$$

where x and y represent the coordinate system in the original element; x_i, y_i are the coordinates of the i^{th} node; and Ψ_i is the basis function of i^{th} node in the transformed element. These kinds of FEM formulation in which same basis functions are used for geometric and field variable approximation are called as isoparametric formulations. Nevertheless, the field variable can now be expressed as

$$u(x,y,z) = u(r,s,t) = \sum_{i=1}^{n} \Psi_i(r,s,t) u_i \tag{2.49}$$

To evaluate the weak form integral, we need to compute $\frac{\partial \Psi_i}{\partial x}$, $\frac{\partial \Psi_i}{\partial y}$, and $\frac{\partial \Psi_i}{\partial z}$. However, Ψ_i is a function of r, s, and t. To compute these derivatives, we must invert the following relations.

$$\frac{\partial \Psi_i}{\partial r} = \frac{\partial \Psi_i}{\partial x}\frac{\partial x}{\partial r} + \frac{\partial \Psi_i}{\partial y}\frac{\partial y}{\partial r} + \frac{\partial \Psi_i}{\partial z}\frac{\partial z}{\partial r} \tag{2.50}$$

$$\frac{\partial \Psi_i}{\partial s} = \frac{\partial \Psi_i}{\partial x}\frac{\partial x}{\partial s} + \frac{\partial \Psi_i}{\partial y}\frac{\partial y}{\partial s} + \frac{\partial \Psi_i}{\partial z}\frac{\partial z}{\partial s} \tag{2.51}$$

$$\frac{\partial \Psi_i}{\partial t} = \frac{\partial \Psi_i}{\partial x}\frac{\partial x}{\partial t} + \frac{\partial \Psi_i}{\partial y}\frac{\partial y}{\partial t} + \frac{\partial \Psi_i}{\partial z}\frac{\partial z}{\partial t} \tag{2.52}$$

$$\begin{Bmatrix} \frac{\partial \Psi_i}{\partial x} \\ \frac{\partial \Psi_i}{\partial y} \\ \frac{\partial \Psi_i}{\partial z} \end{Bmatrix} = \begin{bmatrix} \frac{\partial x}{\partial r} & \frac{\partial y}{\partial r} & \frac{\partial z}{\partial r} \\ \frac{\partial x}{\partial s} & \frac{\partial y}{\partial s} & \frac{\partial z}{\partial s} \\ \frac{\partial x}{\partial t} & \frac{\partial y}{\partial t} & \frac{\partial z}{\partial t} \end{bmatrix}^{-1} \begin{Bmatrix} \frac{\partial \Psi_i}{\partial r} \\ \frac{\partial \Psi_i}{\partial s} \\ \frac{\partial \Psi_i}{\partial t} \end{Bmatrix} \tag{2.53}$$

The 3×3 matrix on the right-hand side is called a Jacobian matrix. To obtain the solution it is imperative for the Jacobian matrix to be non-singular.

2.1.3 Assembly and Solution

As discussed earlier, the field variable for a steady state heat transfer problem can be expressed in terms of basis functions as $T^e(x,y) = \sum_{i=1}^{N} T_i^e \psi_i^e$. Substituting this equation along with the approximation of weight functions $w^e(x,y) = \sum_{j=1}^{N} v_j \psi_j^e$ into the weak form (eqn. 2.5) we get

$$\sum_{i=1}^{n} \left\{ \int_{\Omega^e} \left[\frac{\partial \psi_j^e}{\partial x} \left(k_x \frac{\partial \psi_i^e}{\partial x} \right) + \frac{\partial \psi_j^e}{\partial y} \left(k_y \frac{\partial \psi_i^e}{\partial y} \right) + \frac{\partial \psi_j^e}{\partial z} \left(k_z \frac{\partial \psi_i^e}{\partial z} \right) \right] d\Omega + \oint_{\Gamma^e} h \psi_j^e \psi_i^e \, d\Gamma \right\} v_j T_i^e - \int_{\Omega^e} v_j \psi_j^e Q \, d\Omega - \oint_{\Gamma^e} v_j \psi_j^e q_n \, d\Gamma - \oint_{\Gamma^e} h T_c v_j \psi_j^e \, d\Gamma = 0 \tag{2.54}$$

The above expression must be satisfied for every value of w. Therefore, we need to remove the arbitrariness of w which can be done by making the above expression invariant with respect to w. In this case, the derivative of above expression with respect to v_j should be equal to zero to make the expression invariant with respect to w, giving us the following equation

$$\sum_{i=1}^{n} \left\{ \int_{\Omega^e} \left[\frac{\partial \psi_j^e}{\partial x} \left(k_x \frac{\partial \psi_i^e}{\partial x} \right) + \frac{\partial \psi_j^e}{\partial y} \left(k_y \frac{\partial \psi_i^e}{\partial y} \right) + \frac{\partial \psi_j^e}{\partial z} \left(k_z \frac{\partial \psi_i^e}{\partial z} \right) \right] d\Omega + \oint_{\Gamma^e} h \psi_j^e \psi_i^e \, d\Gamma \right\} T_i^e - \int_{\Omega^e} \psi_j^e Q \, d\Omega - \oint_{\Gamma^e} \psi_j^e q_n \, d\Gamma - \oint_{\Gamma^e} h T_c \psi_j^e \, d\Gamma = 0 \tag{2.55}$$

The above equation can be expressed in simplified form as

$$\sum_{i=1}^{n} K_{ij}^{e} T_i = Q_j^e + q_j^e \tag{2.56}$$

where K_{ij}^{e}, Q_j^e, and q_j^e are:

$$K_{ij}^{e} = \int_{\Omega^e} \frac{\partial \psi_j^e}{\partial x}\left(k_x \frac{\partial \psi_i^e}{\partial x}\right) + \frac{\partial \psi_j^e}{\partial y}\left(k_y \frac{\partial \psi_i^e}{\partial y}\right) + \frac{\partial \psi_j^e}{\partial z}\left(k_z \frac{\partial \psi_i^e}{\partial z}\right) d\Omega + \oint_{\Gamma^e} h \psi_j^e \psi_i^e \, d\Gamma \tag{2.57}$$

$$Q_j^e = \int_{\Omega^e} \psi_j^e Q \, d\Omega \tag{2.58}$$

$$q_j^e = \oint_{\Gamma^e} \psi_j^e q_n \, d\Gamma + \oint_{\Gamma^e} h T_c \psi_j^e \, d\Gamma \tag{2.59}$$

In matrix notation equation 2.59 can be expressed as

$$[K^e]\{T^e\} = \{Q^e\} + \{q^e\} \tag{2.60}$$

where K^e is the element stiffness matrix and $\{Q^e\} + \{q^e\}$ collectively form the force vector. Numerical integration techniques like the Gauss-Legendre quadrature formulas are generally used to evaluate the integrals involved in above expressions, as it is very difficult to evaluate these integrals analytically.

The element stiffness matrix is then assembled into a global matrix. Assembly is based on two basic rules:

1. Continuity of primary variable must be maintained
2. Secondary variable (flux) must be balanced

According to the 1st rule if two elements share a node, then that node must have a unique temperature value. The second rule makes sure that the heat flux is balanced

throughout the domain. Global K, Q, and q are assembled using the element connectivity information. The initial differential equation is now transformed to a set of algebraic equations given by

$$[K]\{T\} = \{F\} \tag{2.61}$$

where $F = Q + q$

After applying the proper boundary conditions, the above system of equations can be solved to get the solution vector $\{T\}$. It can be solved using direct inversion of K matrix or by using iterative methods such as Gauss-Seidel method. For large meshes, the direct method is not feasible, as it requires a huge amount of memory as well as processing power.

2.2. Stochastic Finite Element Method (SFEM)

SFEM incorporates the uncertainty present in the design variables to perform a comprehensive analysis which is more reliable than tradition Finite Element Method. The advantage of SFEM over the conventional statistical method is that it requires information about only the first two moments of the distribution, which are mean and standard deviation respectively [10]. SFEM is computationally more efficient compared to statistical methods like Monte-Carlo simulation which require running a considerably large amount of simulations to study a response variation [4]. SFEM can be broadly categorized into three categories

2.2.1 Spectral Method

Introduced by Ghanem and Spanos [5], the spectral approach represents responses using polynomial chaos expansions and discretize the input random variables using Karhunem-Loeve expansion [6]. The polynomial chaos of a random variable can be expressed as

$$w(\theta) = \sum_{j=0}^{N} w_j \Psi_j \left(\{\Phi_j(\theta)\}_{k=1}^{N}\right) \tag{2.62}$$

where the polynomials $\{\Phi_j(\theta)\}_{k=1}^{N}$ are the orthogonal chaos basis [2]. Because of its complexity and an enormous amount of computational time requirement, this method is not suitable for most practical problems and is generally restricted to 1-D and 2-D linear problems [2,4].

2.2.2 Perturbation Method

The perturbation method employs Taylor series to expand the input random variables about their mean. For a finite element heat transfer problem with KU=F as a system of algebraic equations K, U, and F can be represented as

$$K = K_0 + \sum_{i=1}^{N} a_i \frac{\partial K}{\partial a_i}|_{a=0} + \frac{1}{2}\sum_{i=1}^{N}\sum_{j=1}^{N} a_i a_j \frac{\partial^2 K}{\partial a_i \partial a_j}|_{a=0} + \cdots \tag{2.63}$$

$$U = U_0 + \sum_{i=1}^{N} a_i \frac{\partial U}{\partial a_i}|_{a=0} + \frac{1}{2}\sum_{i=1}^{N}\sum_{j=1}^{N} a_i a_j \frac{\partial^2 U}{\partial a_i \partial a_j}|_{a=0} + \cdots \tag{2.64}$$

$$F = F_0 + \sum_{i=1}^{N} a_i \frac{\partial F}{\partial a_i}|_{a=0} + \frac{1}{2}\sum_{i=1}^{N}\sum_{j=1}^{N} a_i a_j \frac{\partial^2 F}{\partial a_i \partial a_j}|_{a=0} + \cdots \qquad (2.65)$$

where K_0, F_0, and U_0 are the mean values and a_i are the random variables. The accuracy increases with the inclusion of higher order terms; however, it increases the computational cost [7].

2.2.3 Probabilistic Approach

In this approach, the randomness of the input variables is characterized by their means, standard deviations, and corresponding probability density functions. The main focus is on computing the probability of failure using some performance criterion described by an equation called limit state equation. For example, the probability of failure of a system can be expressed as

$$p_f = \int \dots \int_{g(\,)<0} f_X(x_1, x_2, \dots, x_n) dx_1 dx_2 \dots dx_n \qquad (2.66)$$

where f_X is the joint probability density function (PDF) of the random variables $X_1, X_2, \dots X_n$ and g( ) is the limit state function for the system. Figure 2.7 shows the joint probability density function and failure and safe regions for a model involving two random variables. The net volume under the joint PDF is the total probability for the system. The volume covering the failure region is the probability of failure for the system. The PDF of a standard normal distribution is given by

$$f_z(z) = \frac{1}{\sqrt{2\pi}} e^{\left(-\frac{1}{2}z^2\right)} \qquad (2.67)$$

If we assume that all the random variables are uncorrelated, then the joint PDF can be given by the following expression

$$f_Z(z_1, z_2 \dots z_n) = \prod_{i=1}^{n} \frac{1}{\sqrt{2\pi}} e^{\left(-\frac{1}{2}z_i^2\right)} \tag{2.68}$$

Assuming uncorrelated variables, the probability of failure can be expressed as

$$p_f = \int \dots \int_{g(\,)<0} \prod_{i=1}^{n} \frac{1}{\sqrt{2\pi}} e^{\left(-\frac{1}{2}z_i^2\right)} dz_1 dz_2 \dots dz_n \tag{2.69}$$

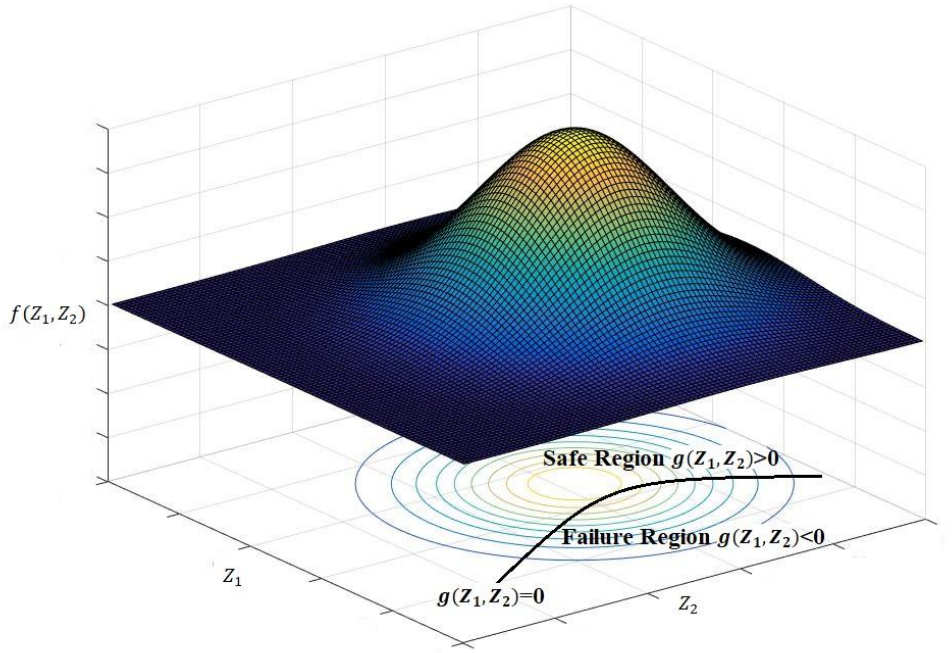

Figure 2.7 Joint PDF for a model with two random variables

2.3 Probabilistic Approach to Stochastic Finite Element Method

As mentioned in the previous section, to determine the probability of failure we must define a proper limit state function and information of joint probability function is also required beforehand. In general, computing the integral in equation 2.66 is very complicated especially for real-world problems with non-linear limit state function [1].

2.3.1 Limit State Function

Limit state function defines the criterion which needs to be satisfied for a reliable design. If S and R are the load and resistance distributions respectively, then limit state function is a function of S and R; i.e. g(R, S). Limit state function defines the failure and safe region within the design domain. It can be implicit or explicit, linear or non-linear in nature. Failure region and safe regions are mathematically defined by g( )<0 and g( )>0 respectively. The curve shown in figure 2.7 depicts the failure and safe region.

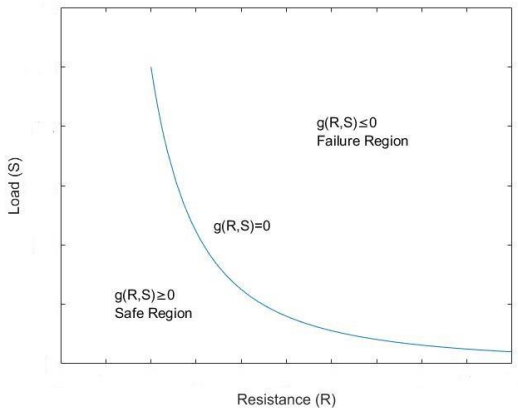

Figure 2.8 Limit State Curve

Limit state function provides constraint function for determining the probability of failure. Determining the integral in Eqn. 2.66 in is called the full distribution approach. Evaluating it requires the information of joint probability density function which is almost impossible to obtain for real-world problems [1]. Furthermore, it is very complicated to compute the integral even if the information of joint probability density function is available. Several methods exist to approximately compute the integral, which can be broadly grouped into two classes: First-Order Reliability Methods and Second-Order Reliability Methods. Only first-order reliability method is discussed in this thesis.

2.3.2 First Order Reliability Method (FORM)

First-order reliability method is developed from the second-moment method which uses information of first and second moment of the random variables [1]. The first and second moments are simply the mean and standard deviation of the distribution.

Since for most real-life problems limit state function is non-linear, FORM can be used to linearize the limit state function and approximately compute the probability of failure. It linearizes the limit state function at the most probable point (MPP) of failure in the transformed standard normal space Z using Rosenblatt transformation [8].

$$g(X) = g(Z) \cong g(z^*) + \nabla \mathrm{g}^{\mathrm{T}}(Z - z^*) \tag{2.70}$$

Where z^* is the most probable point of failure. It is the nearest point from the origin that lies on the limit state curve. The distance of MPP from the origin is called

reliability index β. To find the MPP, we need to find the design points for which joint PDF is maximum on the limit state surface. In other words, we need to maximize the term $\prod_{i=1}^{n} \frac{1}{\sqrt{2\pi}} e^{\left(-\frac{1}{2}z_i^2\right)}$ in equation 2.69 while satisfying the constraint g( )=0, which is same as minimizing the term $\sum_{i=1}^{n} \sqrt{z_i^2}$. The term $\sum_{i=1}^{n} \sqrt{z_i^2}$ represents the distance of design point z, which lies on the limit state curve, from the origin. The MPP search now becomes the following optimization problem

$$minimize\ ||z||$$

$$subject\ to\ g(Z) = 0$$

Where g(Z) is the limit state function in the transformed standard normal space. Rackwitz and Fiessler [9] developed a FORM algorithm which utilizes Newton-Raphson method to find the design point. The steps in the algorithm are:

1. Define limit state function.
2. Assume initial reliability index β_0 and initial values for design points $x_i, i = 1, 2, 3, \ldots n$ and compute the limit state function $g( )$.
3. Transform the design points to equivalent standard normal space by

$$z_i = \frac{x_i - \mu_{X_i}^N}{\sigma_{X_i}^N} \tag{2.71}$$

   where $\mu_{X_i}^N$ and $\sigma_{X_i}^N$ are the mean and standard deviation of ith design point in the normal space.
4. Evaluate $\frac{\partial g}{\partial Z_i}$ at the design points. $\frac{\partial g}{\partial Z_i}$ can also be expressed as $\frac{\partial g}{\partial X_i}\sigma_{X_i}^N$

5. Evaluate new design points in equivalent standard normal space by

$$z^{k+1} = \frac{1}{|\nabla g(z^k)|^2}\left[\nabla g(z^k)^T z^k - g(z^k)\right]\nabla g(z^k) \tag{2.72}$$

6. Compute reliability index using following equation and check for convergence

$$\beta = \sqrt{\sum_{i=1}^{n} z_i^2} \tag{2.73}$$

7. Update design points in original coordinate using

$$x_i = z_i * \sigma_{X_i}^N + \mu_{X_i}^N \tag{2.74}$$

and compute limit state function using updated design points. Also, check for convergence of $g(\,) = 0$

8. Repeat steps 3 to 7 if converge criterion is not met for $g(\,)$ and β.

2.4 Sensitivities Calculation

The simplest method to calculate sensitivity is through finite-difference method (FDM). According to FDM, the sensitivity of a function f with respect to a variable x is given by

$$\frac{\partial f}{\partial x} = \frac{f(x + \Delta x) - f(x - \Delta x)}{2\Delta \mathrm{x}} \tag{2.75}$$

FDM is prone to cancellation errors that can arise if the step-size is too small or too big [11] [12]. It is very difficult to find the correct step size for FDM for complex

problems which include several parameters. Also, if the range of values of parameters is very large a single value of perturbation would not work. In that case, correct step size for every parameter would need to be found separately.

In the Complex variable method (CVM) the results obtained are accurate, however, it requires a large amount of computational time and memory [2] [11] [12]. The sensitivity of a function f using CVM is given by

$$\frac{\partial f}{\partial x} = \frac{Im\big(f(x + \Delta x)\big)}{\Delta x} \tag{2.76}$$

Semi-analytic method (SAM) has higher efficiency than FDM, however, it also suffers from cancellation error like FDM. In SAM, for a finite element formulation $KU = F$, the sensitivity of U with respect to a variable x is given by

$$\frac{\partial U}{\partial x} = K^{-1}\left(\frac{\partial F}{\partial x} - U\frac{\partial K}{\partial x}\right) \tag{2.77}$$

SACVM combines the efficiency of semi-analytic method and accuracy of the complex variable method. The only difference between SAM and SACVM is the way in which $\frac{\partial K}{\partial x}$ and $\frac{\partial F}{\partial x}$ are calculated. In SACVM $\frac{\partial K}{\partial x}$ and $\frac{\partial F}{\partial x}$ are calculated using complex-variable method by perturbing the force vector and stiffness matrix in the complex direction.

$$\frac{\partial K}{\partial x} = \frac{Im\big(K(x + \Delta x)\big)}{\Delta x} \tag{2.78}$$

$$\frac{\partial F}{\partial x} = \frac{Im\big(F(x + \Delta x)\big)}{\Delta x} \tag{2.79}$$

Jin et al [12] have shown that SACVM is insensitive to step size and can provide accurate sensitivity information. Grisham et al [11] used SACVM to calculate sensitivities in heat transfer problems. Previous researchers have implemented SACVM for obtaining effective thermal conductivity [15,16,17]. In this study, SACVM and FDM are used to calculate the sensitivity of limit state function with respect to the random variables.

Chapter 3 METHODOLOGY

3.1 BGA Package

3.1.1 Geometry

A simplified geometry was chosen to solve the problem. The dimension of printed wire board, package, and die are 30mm×30mm, 13mm×13mm, and 7.2mm×7.2mm respectively. This model does not include the intricate circuitry of the chip; however, it includes simplified regions which are reasonable enough to perform the thermal analysis. The geometry is symmetric about x and y-axis, therefore only $1/4^{th}$ of it is modeled to save computational time. The figure below depicts each region in the geometry.

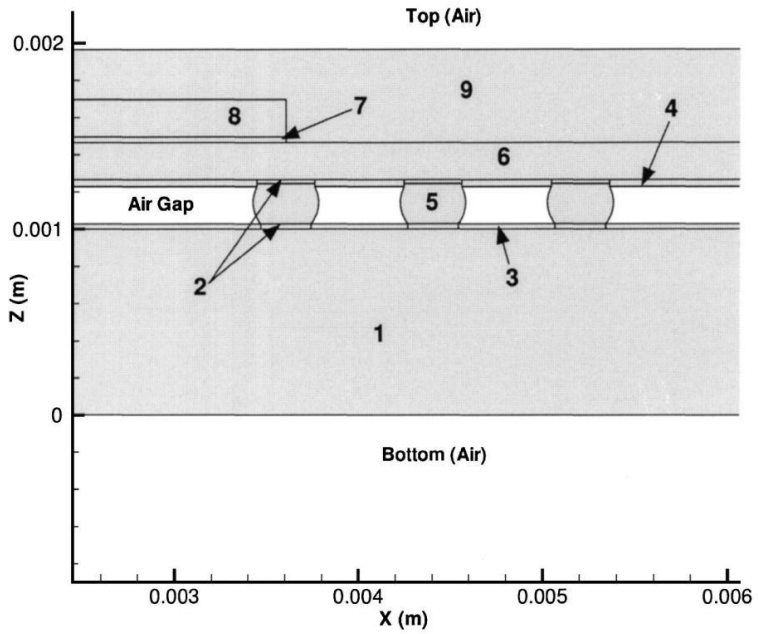

Figure 3.1 Cross-Sectional View of BGA Package [3]

The geometry is made of 9 different material domains. Information about the mean and standard deviation of their conductivities are listed in table 3.1. For convenience, standard deviations are chosen to be 10% of mean values for each material.

Table 3.1 Mean and Standard Deviation of Material Thermal Conductivities

Material Region	Material	Mean value of Conductivities	Standard deviation of conductivities
1	Printed Wire Board	1.0	0.1
2	Copper Pads	393.0	39.3
3	Solder Masks	0.2	0.02
4	Polyimide Tape	0.3	0.03
5	Solder Balls	250	25
6	BT Substrate	1.0	0.1
7	Die Attach	0.25	0.025
8	Silicon Die	87.0	8.7
9	Epoxy Mold Compound	0.71	0.071

Die is treated as a heat source with a mean value of power density as Q= 7.65×10^7 W/m^3 and standard deviation of 7.65×10^6 W/m^3. Heat transfer coefficient(h) and ambient temperature(T_{amb}) values are also uncertain. h has a mean value of 20 W/m^2-℃ and standard deviation value of 2 W/m^2-℃, T_{amb} has a mean value of 25℃ and standard deviation value of 2.5℃.

3.1.2 Mesh

As mentioned earlier, taking advantage of symmetry in geometry only 1/4th of the model is created to save computational time. Mesh is shown in fig. 3.2.

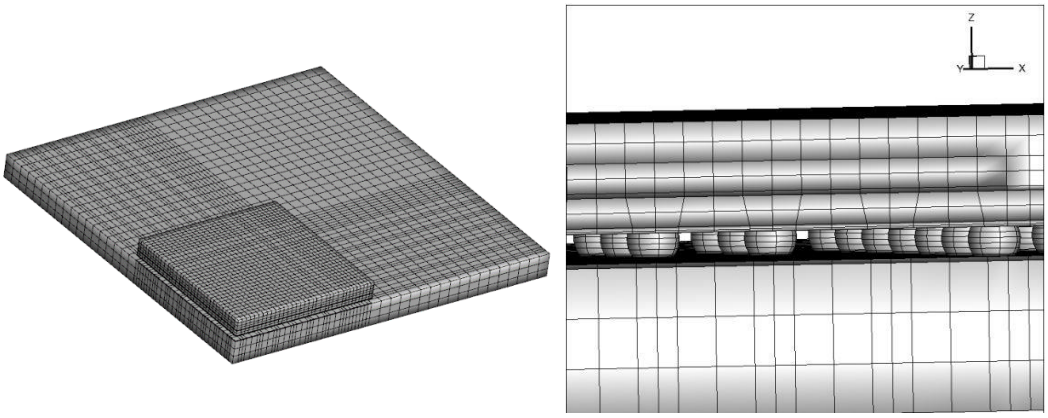

(a) (b)

Figure 3.2 (a) Mesh of the 1/4th BGA model (b) Close-up View of Mesh

The summary of the number of nodes and types of elements is shown in table 3.2

Table 3.2 Summary of Mesh

Number of nodes	27417
Number of boundary triangles	0
Number of boundary quads	12608
Number of tetrahedral cells	0
Number of pyramid cells	0
Number of prism cells	0
Number of hexahedral cells	20728

3.1.3 Stochastic Finite Element Formulation

Galerkin's Finite Element, as discussed in section 2.1.1 is used for this problem. Following assumptions are made to simplify the problem:

1. Thermal conductivities of all the materials are constant and same in all directions
2. The solution is invariant with time (steady state)
3. Source term is constant
4. There is no thermal contact resistance between the interface of two materials
5. All distributions are Gaussian distributions

Governing equation for the problem is given by

$$\frac{\partial}{\partial x}\left(k\frac{\partial T}{\partial x}\right)+\frac{\partial}{\partial y}\left(k\frac{\partial T}{\partial y}\right)+\frac{\partial}{\partial z}\left(k\frac{\partial T}{\partial z}\right)+Q=0 \qquad (3.1)$$

and the boundary conditions are:

1. Convective BC on all sides of PWB with $h=20\frac{W}{m^{2}℃}$ and $T_{\infty}=25℃$
2. Convective BC on top, bottom, and sides of the package with $h=20\frac{W}{m^{2}℃}$ and $T_{\infty}=25℃$
3. Symmetry BC on symmetric sides, $\frac{dT}{dn}=0$
4. Zero heat flux on sides of solder balls, $\frac{dT}{dn}=0$

Using the method discussed in chapter 2, the element stiffness matrix and force function for this problem can be written as

$$K_{ij}^{e} = \int_{\Omega^e} k\left(\frac{\partial \psi_j^e}{\partial x}\frac{\partial \psi_i^e}{\partial x} + \frac{\partial \psi_j^e}{\partial y}\frac{\partial \psi_i^e}{\partial y} + \frac{\partial \psi_j^e}{\partial z}\frac{\partial \psi_i^e}{\partial z}\right) d\Omega + \oint_{\Gamma^e} h\psi_j^e \psi_i^e \, d\Gamma \tag{3.2}$$

$$F_{ij}^{e} = \int_{\Omega^e} \psi_j^e Q \, d\Omega + \oint_{\Gamma^e} hT_\infty \psi_j^e \, d\Gamma \tag{3.3}$$

It must be noted that for inner elements second terms in both K_{ij}^{e} and F_{ij}^{e} goes to zero. It is only non-zero for boundary elements. Collectively these algebraic equations can be written as

$$K^e T^e = F^e \tag{3.4}$$

These stiffness matrices are then assembled into a global matrix to solve for nodal temperatures.

To perform stochastic analysis, we use FORM as discussed in section 2.3.2. The limit state function is chosen as $g(\,) = T_{avg} - 97$, where T_{avg} is the average temperature at the interface of die and heat-spreader. This limit state function is chosen because the die-junction temperature is crucial in electronics design and excessive temperature at the interface is generally a cause of failure. To calculate reliability index, we need to compute sensitivity of limit state function with respect to random variables; material conductivities and source power density in this case. The flow chart of the algorithm for reliability analysis using SACVM is shown below

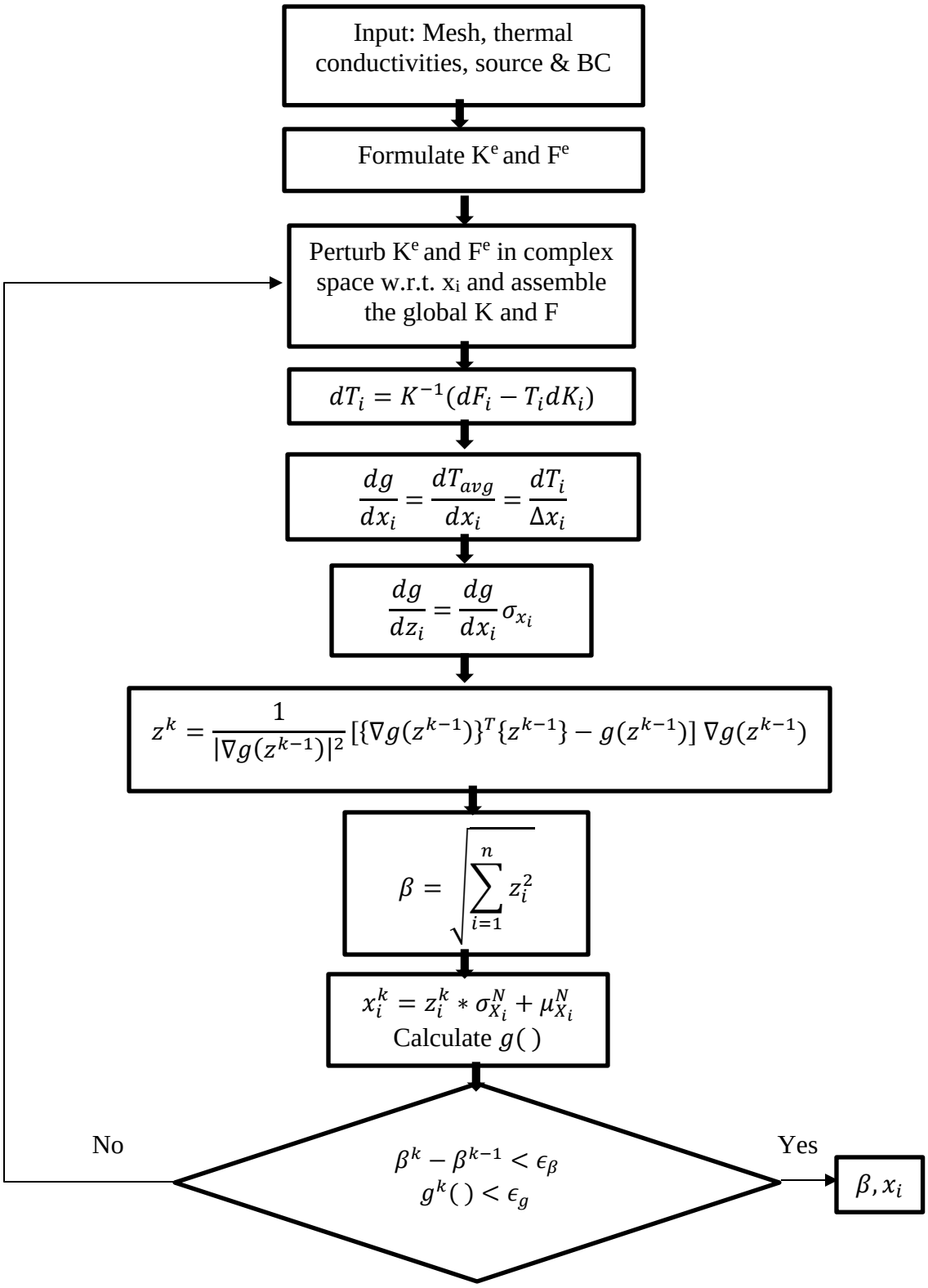

Figure 3.3 Flowchart of FORM using SACVM

Where k is the iteration number, ϵ_β and ϵ_g are equal to 10^{-3}, and x represents the random variable. While using FDM, the only difference is in calculating the sensitivities of limit state function. In FDM it can be calculated as

$$\frac{\partial g}{\partial x} = \frac{g(x + \Delta x) - g(x - \Delta x)}{2\Delta x} \tag{3.5}$$

The procedure mentioned above was used to study how the probability of failure changes with a change in standard deviation of random variables. The probability of failure can then be calculated using the following equation.

$$p_f = 1 - \Phi(\beta) \tag{3.6}$$

where β is the reliability index and Φ is the cumulative density function(CDF). For a standard normal distribution CDF can be calculated as

$$\Phi(s) = \int_{-\infty}^{s} \frac{1}{\sqrt{2\pi}} e^{\left(-\frac{1}{2}s^2\right)} ds \tag{3.7}$$

Chapter 4 RESULTS

The temperature contours of the package are shown in figure 4.1. The average temperature at the interface was calculated to be 88.14℃, which is below the 97℃ limit that we have chosen. Hence, our design is safe. But the question is, how safe?

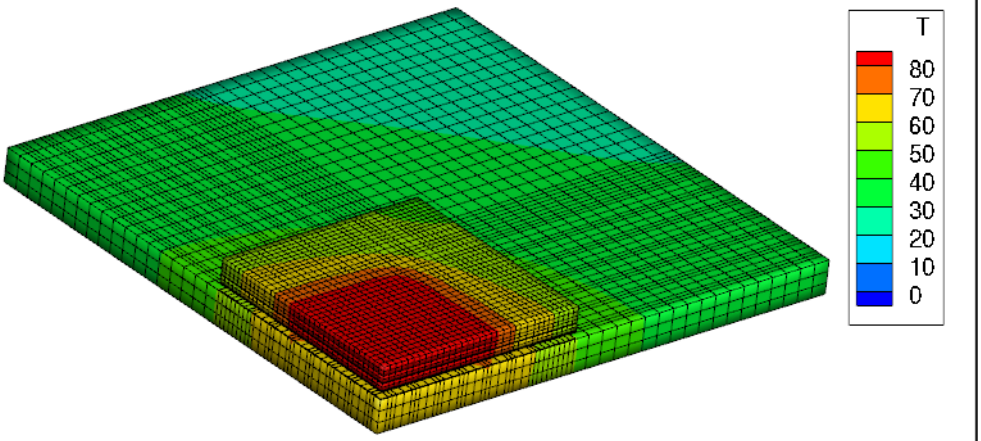

Figure 4.1 Temperature contours (℃)

Two different cases were studied to see the trend of the probability of failure with respect to uncertainties present in the system. In case-1 all 9 material conductivities and heat source are uncertain, whereas in case-2 heat transfer coefficient and ambient temperature are also uncertain. All the uncertainties are assumed to have a Gaussian distribution.

4.1 Case-1: Heat Source and Material Thermal Conductivities are Uncertain

In this case, only heat source and material thermal conductivities are treated as random variables in reliability index calculations. Finite-difference method and SACVM are used to calculate the sensitivity of the limit state function with respect to random variables. For our design values, the probability of failure of the package was calculated to be 0.0015% and the failure points are listed in table 4.1.

Table 4.1 Failure points for Case 1

k1	**k2**	**k3**	**k4**	**k5**	**k6**	**k7**	**k8**	**k9**	**Q**
0.658	392.9	0.199	0.298	249.8	0.859	0.247	85.2	0.572	7.65E7

The trends of the probability of failure with respect to the standard deviations of the random variables using SACVM and FDM are shown in figures below.

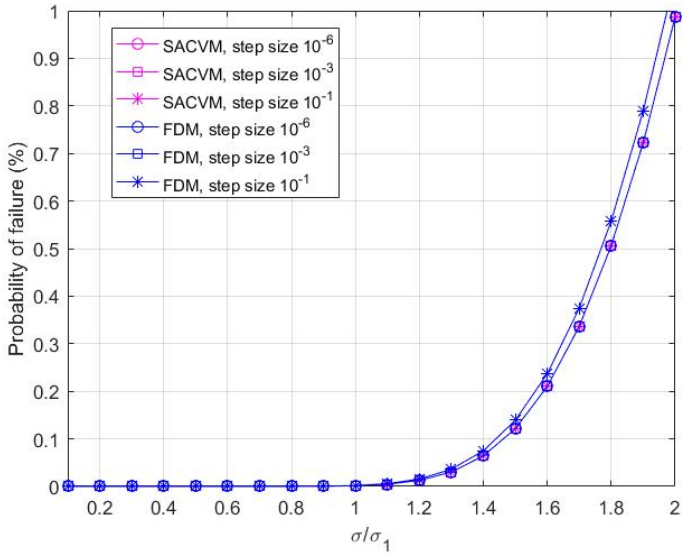

(a)

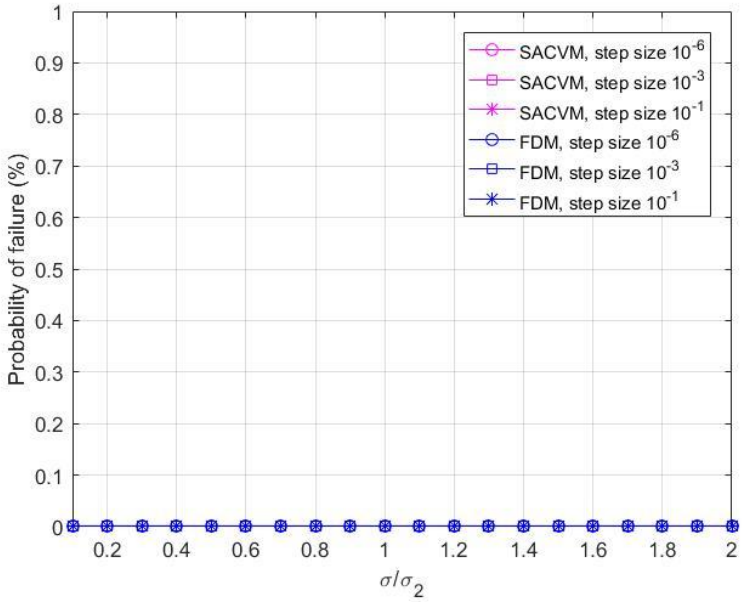
SACVM, step size 10^{-6}
SACVM, step size 10^{-3}
SACVM, step size 10^{-1}
FDM, step size 10^{-6}
FDM, step size 10^{-3}
FDM, step size 10^{-1}
Probability of failure (%)
0
0.1
0.2
0.3
0.4
0.5
0.6
0.7
0.8
0.9
1
0.2
0.4
0.6
0.8
1
1.2
1.4
1.6
1.8
2
σ/σ_2

(b)

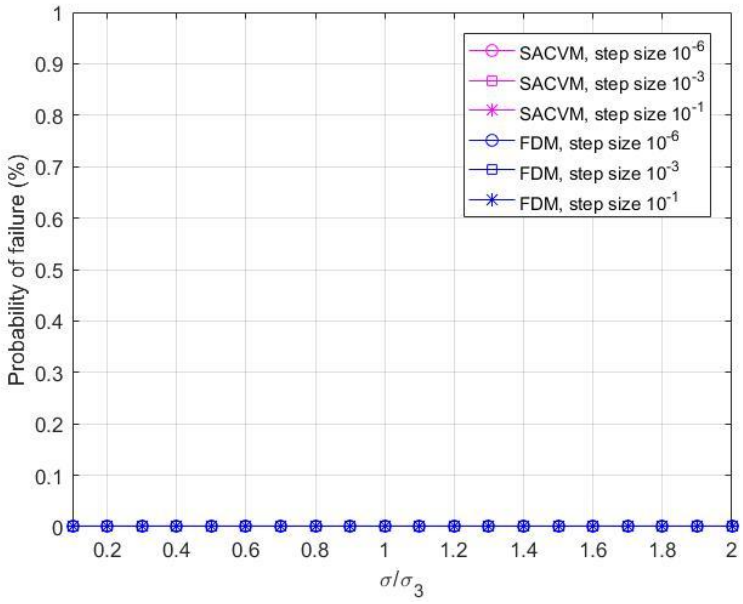
SACVM, step size 10^{-6}
SACVM, step size 10^{-3}
SACVM, step size 10^{-1}
FDM, step size 10^{-6}
FDM, step size 10^{-3}
FDM, step size 10^{-1}
Probability of failure (%)
0
0.1
0.2
0.3
0.4
0.5
0.6
0.7
0.8
0.9
1
0.2
0.4
0.6
0.8
1
1.2
1.4
1.6
1.8
2
σ/σ_3

(c)

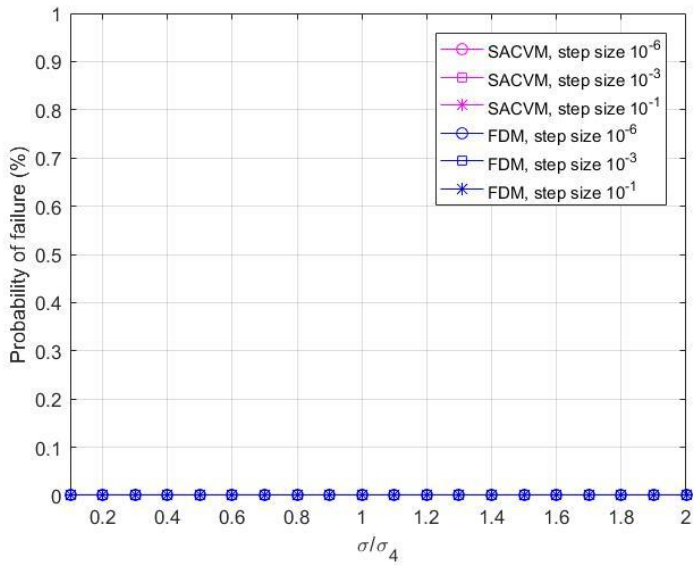
SACVM, step size 10^-6
SACVM, step size 10^-3
SACVM, step size 10^-1
FDM, step size 10^-6
FDM, step size 10^-3
FDM, step size 10^-1
Probability of failure (%)
0
0.1
0.2
0.3
0.4
0.5
0.6
0.7
0.8
0.9
1
0.2
0.4
0.6
0.8
1
1.2
1.4
1.6
1.8
2
σ/σ4

(d)

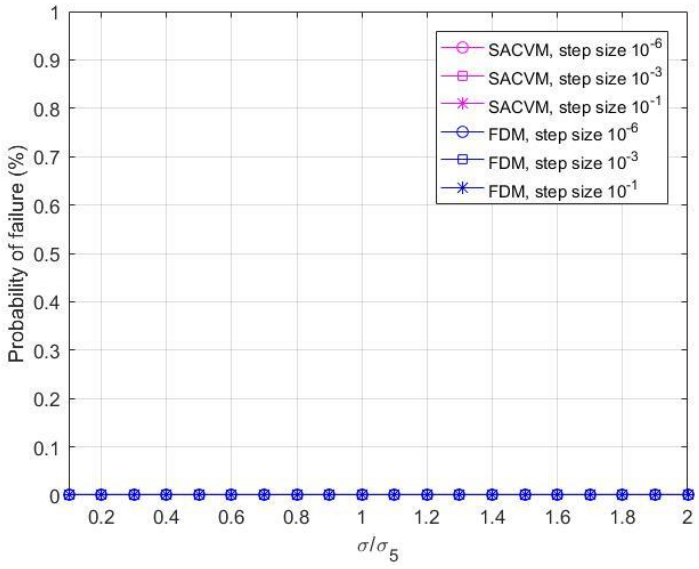
SACVM, step size 10^-6
SACVM, step size 10^-3
SACVM, step size 10^-1
FDM, step size 10^-6
FDM, step size 10^-3
FDM, step size 10^-1
Probability of failure (%)
0
0.1
0.2
0.3
0.4
0.5
0.6
0.7
0.8
0.9
1
0.2
0.4
0.6
0.8
1
1.2
1.4
1.6
1.8
2
σ/σ5

(e)

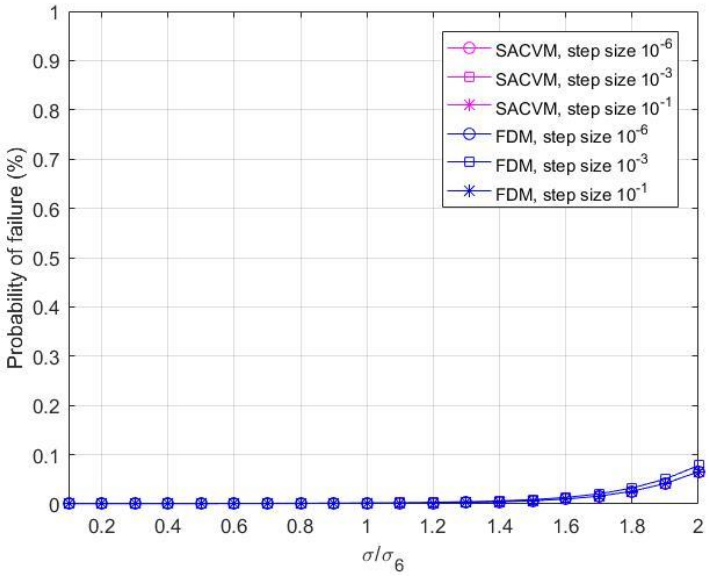
SACVM, step size 10^-6
SACVM, step size 10^-3
SACVM, step size 10^-1
FDM, step size 10^-6
FDM, step size 10^-3
FDM, step size 10^-1
Probability of failure (%)
0
0.1
0.2
0.3
0.4
0.5
0.6
0.7
0.8
0.9
1
0.2
0.4
0.6
0.8
1
1.2
1.4
1.6
1.8
2
σ/σ6

(f)

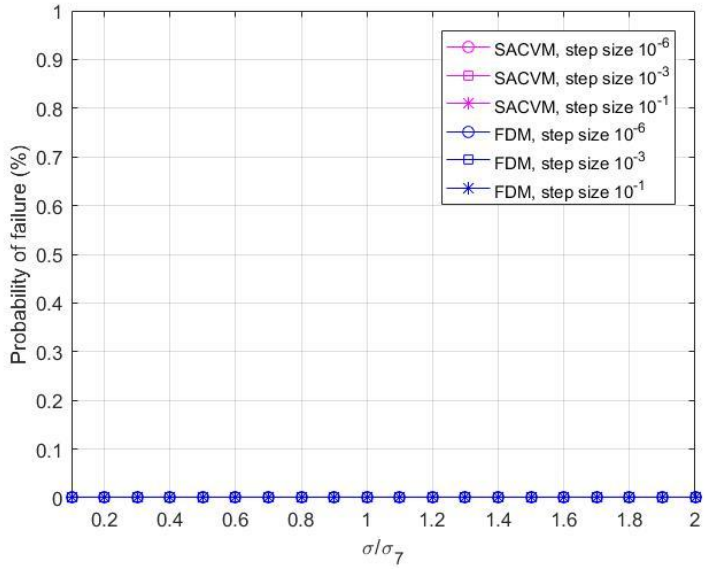
SACVM, step size 10^-6
SACVM, step size 10^-3
SACVM, step size 10^-1
FDM, step size 10^-6
FDM, step size 10^-3
FDM, step size 10^-1
Probability of failure (%)
0
0.1
0.2
0.3
0.4
0.5
0.6
0.7
0.8
0.9
1
0.2
0.4
0.6
0.8
1
1.2
1.4
1.6
1.8
2
σ/σ7

(g)

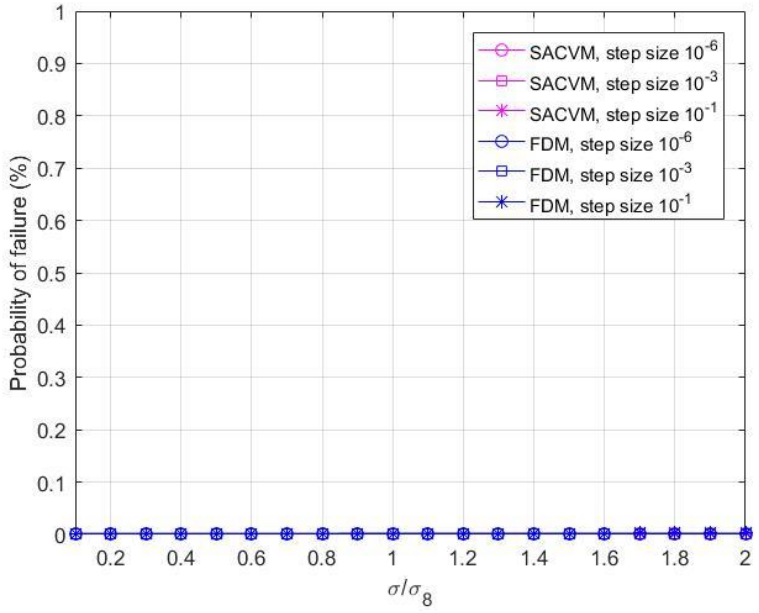
SACVM, step size 10^-6
SACVM, step size 10^-3
SACVM, step size 10^-1
FDM, step size 10^-6
FDM, step size 10^-3
FDM, step size 10^-1
Probability of failure (%)
0
0.1
0.2
0.3
0.4
0.5
0.6
0.7
0.8
0.9
1
0.2
0.4
0.6
0.8
1
1.2
1.4
1.6
1.8
2
σ/σ8

(h)

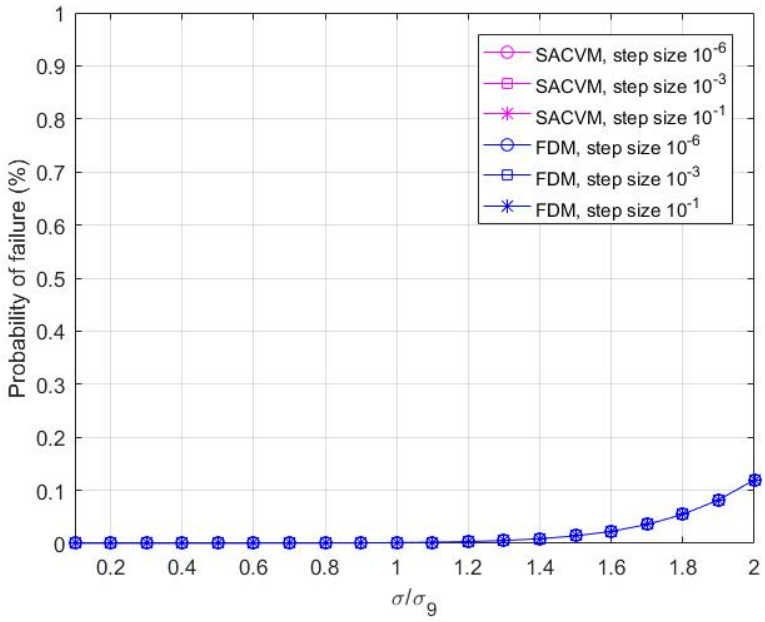
SACVM, step size 10^-6
SACVM, step size 10^-3
SACVM, step size 10^-1
FDM, step size 10^-6
FDM, step size 10^-3
FDM, step size 10^-1
Probability of failure (%)
0
0.1
0.2
0.3
0.4
0.5
0.6
0.7
0.8
0.9
1
0.2
0.4
0.6
0.8
1
1.2
1.4
1.6
1.8
2
σ/σ9

(i)

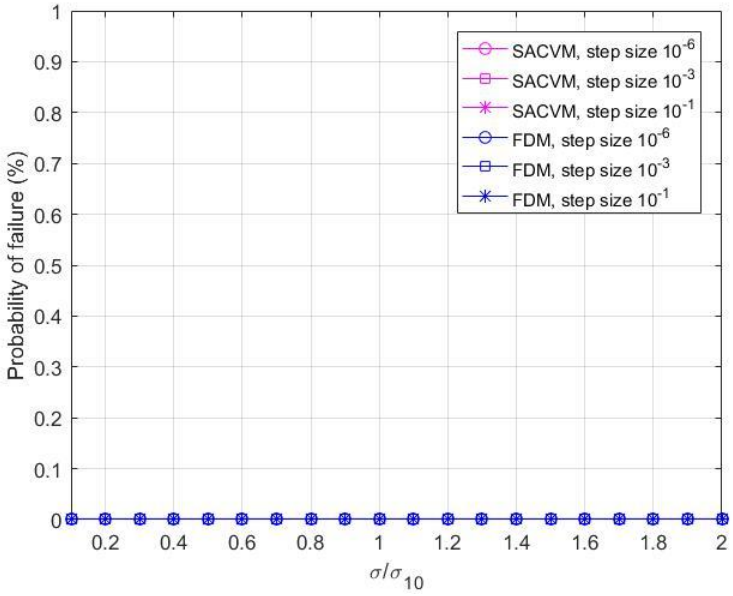

(j)

Figure 4.2 For Case 1, Probability of failure Vs Standard Deviation of random variables (normalized with their original values (a) PWB (b) Copper Pads (c) Solder Mask (d) Polyimide Tape (e) Solder Balls (f) BT Substrate (g) Die Attach (h) Silicon Die (i) Epoxy Mold Compound (j) Heat Source

It can be observed that the probability of failure is particularly sensitive to the thermal conductivity of PWB and a little sensitive to the thermal conductivity of BT substrate and Epoxy mold compound. For every other random variable, the probability of failure doesn't show any sensitivity in the chosen range of standard deviation. Table 4.2 shows the values of probability of failure obtained by using SACVM and FDM using different step sizes. FDM performed similar to SACVM, except for step sizes below or equal to the value of 10^{-8} where convergence could not be obtained.

Table 4.2 Comparison of FDM and SACVM in calculating the probability of failure (CASE 1)

Step Size	**Probability of Failure**	
	SACVM	**FDM**
10^{-1}	0.0015	0.0019
10^{-3}	0.0015	0.0015
10^{-6}	0.0015	0.0015
10^{-8}	0.0015	-
10^{-10}	0.0015	-

4.2 Case 2: Thermal Conductivities, Heat Source, Heat Transfer Coefficient and Ambient Temperature are Uncertain

In this case, in addition to the heat source and thermal conductivities, heat transfer coefficient and ambient temperature are also considered as random variables and have uncertainties present in their values. The probability of failure of our design for this case was calculated to be 2.22% and the failure points are listed in table 4.3. Figure 4.3 shows the variation of p_f with respect to standard deviations for different step sizes using FDM and SACVM.

Table 4.3 Failure points for Case 2

k1	k2	k3	k4	k5	k6	k7	k8	k9	Q	h	T_{amb}
0.953	393	0.199	0.299	250	0.980	0.249	86.7	0.692	7.65E7	16.16	25.44

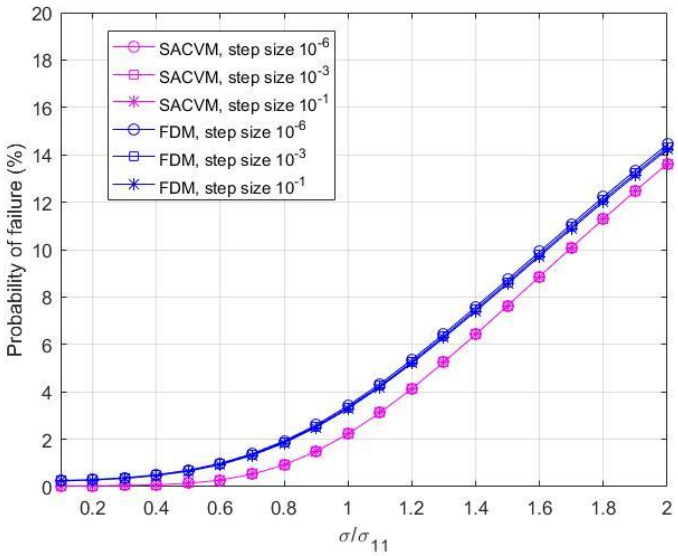

(a)

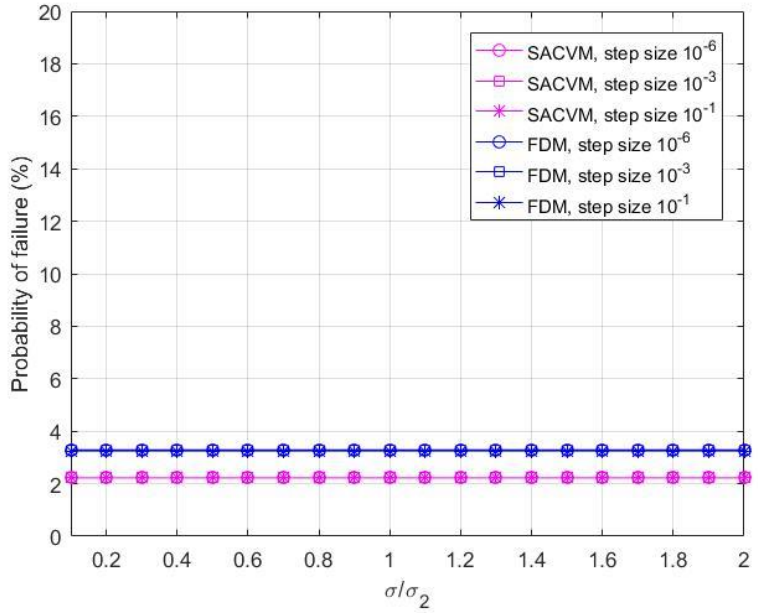
SACVM, step size 10^-6
SACVM, step size 10^-3
SACVM, step size 10^-1
FDM, step size 10^-6
FDM, step size 10^-3
FDM, step size 10^-1
Probability of failure (%)
σ/σ2

(b)

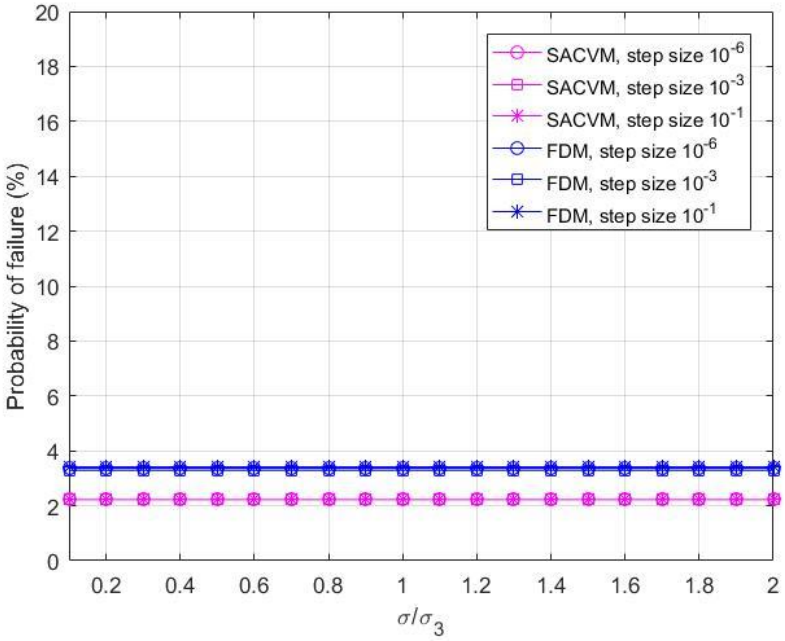
SACVM, step size 10^-6
SACVM, step size 10^-3
SACVM, step size 10^-1
FDM, step size 10^-6
FDM, step size 10^-3
FDM, step size 10^-1
Probability of failure (%)
σ/σ3

(c)

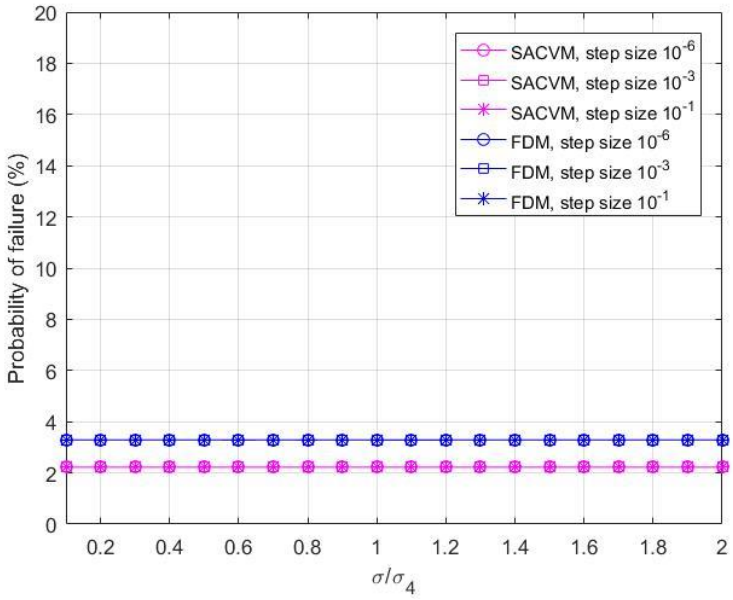
SACVM, step size 10^-6
SACVM, step size 10^-3
SACVM, step size 10^-1
FDM, step size 10^-6
FDM, step size 10^-3
FDM, step size 10^-1
Probability of failure (%)
σ/σ4

(d)

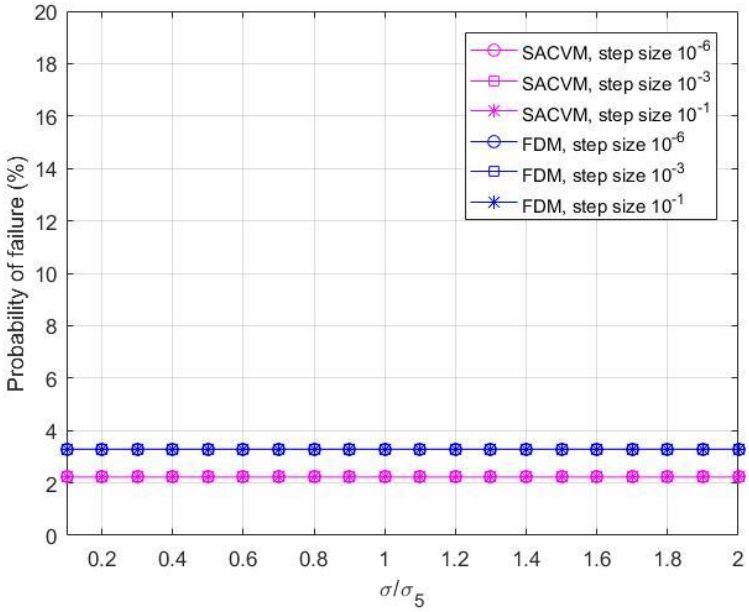
SACVM, step size 10^-6
SACVM, step size 10^-3
SACVM, step size 10^-1
FDM, step size 10^-6
FDM, step size 10^-3
FDM, step size 10^-1
Probability of failure (%)
σ/σ5

(e)

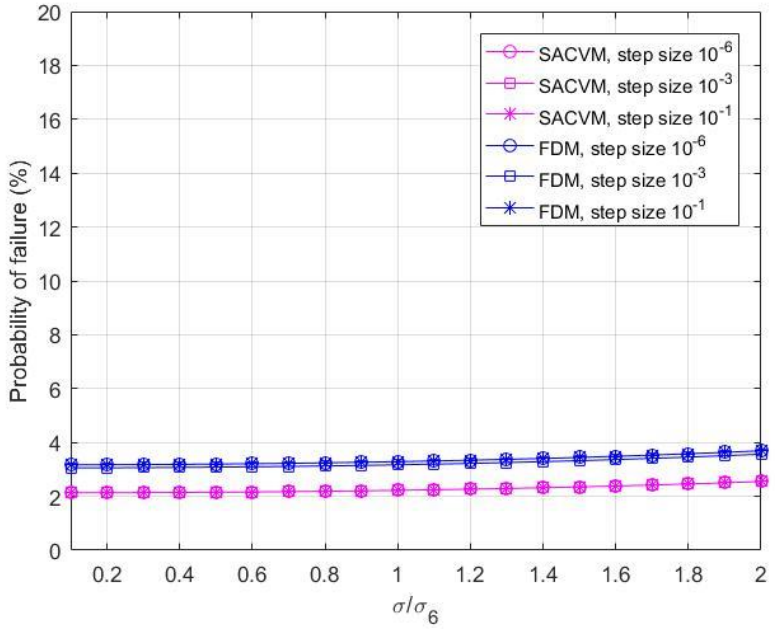
Probability of failure (%)
σ/σ_6
SACVM, step size 10^{-6}
SACVM, step size 10^{-3}
SACVM, step size 10^{-1}
FDM, step size 10^{-6}
FDM, step size 10^{-3}
FDM, step size 10^{-1}

(f)

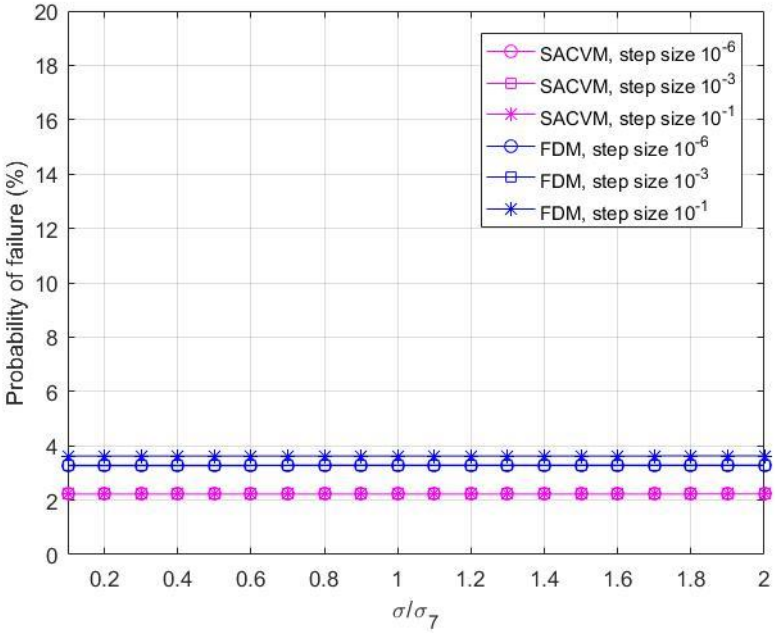
Probability of failure (%)
σ/σ_7
SACVM, step size 10^{-6}
SACVM, step size 10^{-3}
SACVM, step size 10^{-1}
FDM, step size 10^{-6}
FDM, step size 10^{-3}
FDM, step size 10^{-1}

(g)

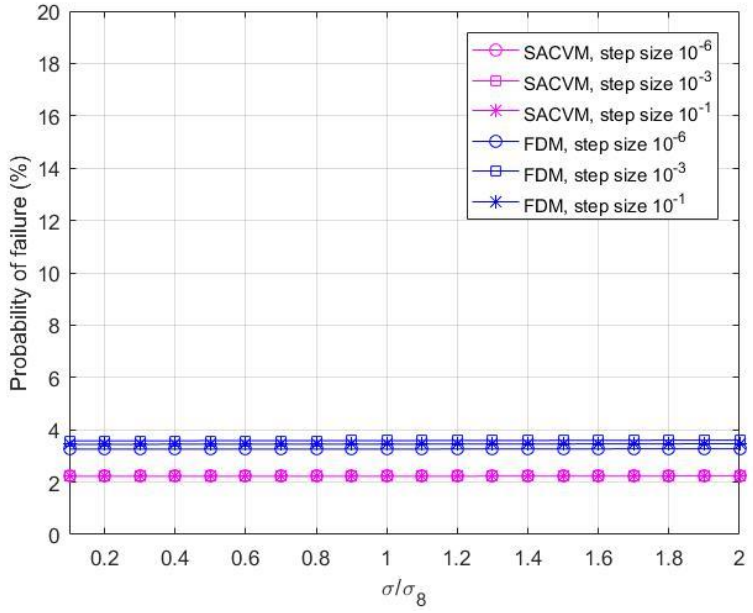
SACVM, step size 10^{-6}
SACVM, step size 10^{-3}
SACVM, step size 10^{-1}
FDM, step size 10^{-6}
FDM, step size 10^{-3}
FDM, step size 10^{-1}
Probability of failure (%)
σ/σ_8

(h)

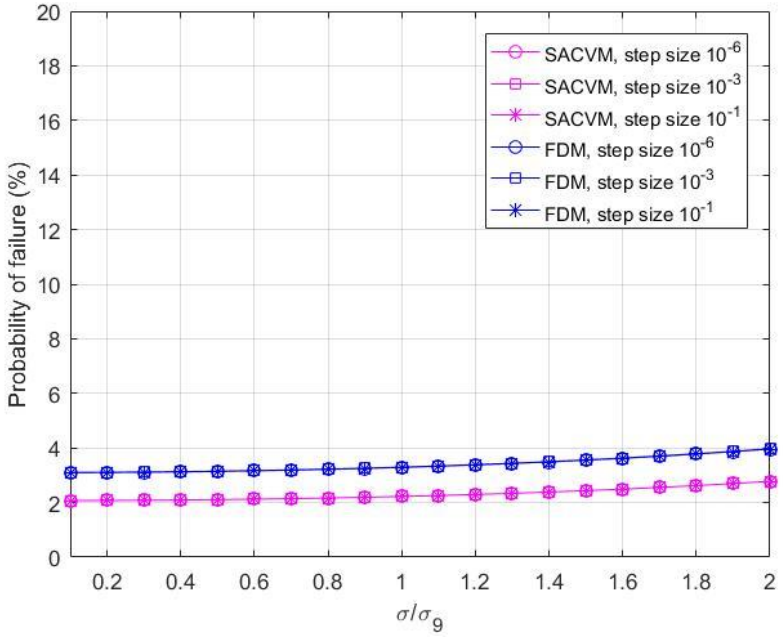
SACVM, step size 10^{-6}
SACVM, step size 10^{-3}
SACVM, step size 10^{-1}
FDM, step size 10^{-6}
FDM, step size 10^{-3}
FDM, step size 10^{-1}
Probability of failure (%)
σ/σ_9

(i)

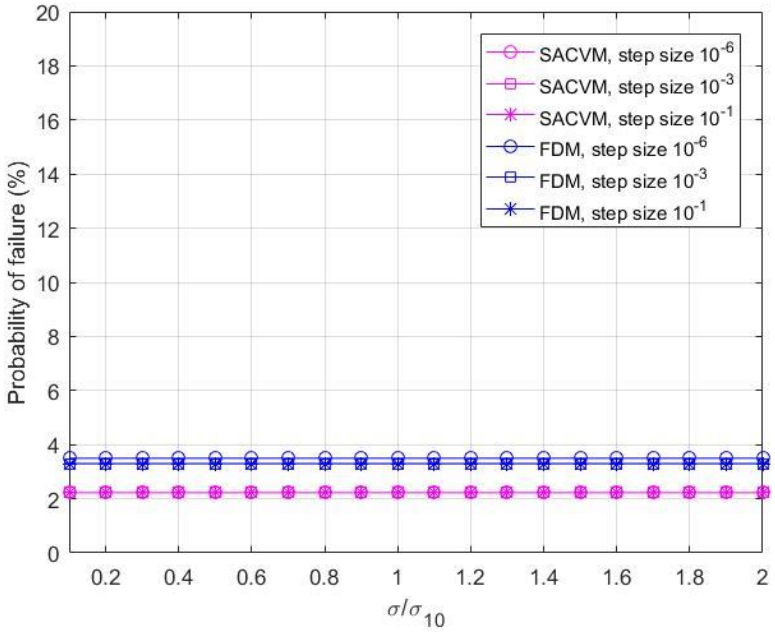
SACVM, step size 10^-6
SACVM, step size 10^-3
SACVM, step size 10^-1
FDM, step size 10^-6
FDM, step size 10^-3
FDM, step size 10^-1
Probability of failure (%)
σ/σ10

(j)

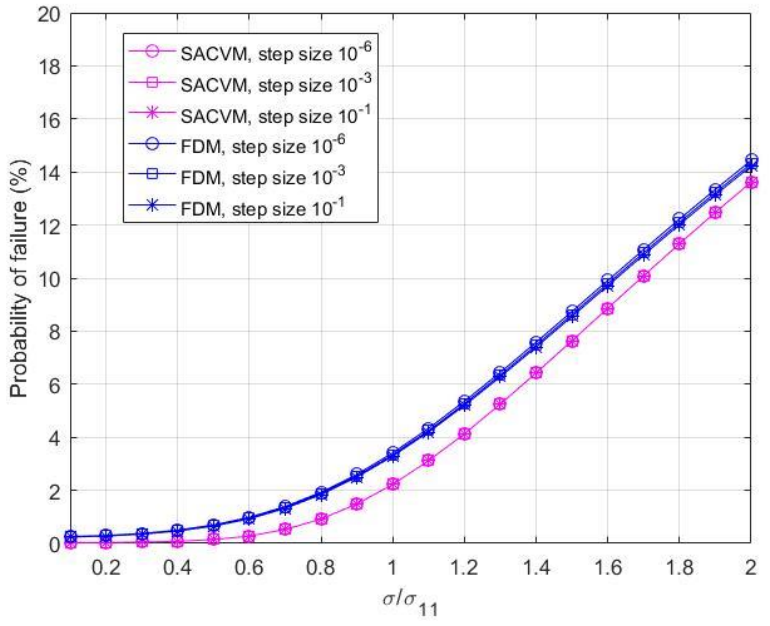
SACVM, step size 10^-6
SACVM, step size 10^-3
SACVM, step size 10^-1
FDM, step size 10^-6
FDM, step size 10^-3
FDM, step size 10^-1
Probability of failure (%)
σ/σ11

(k)

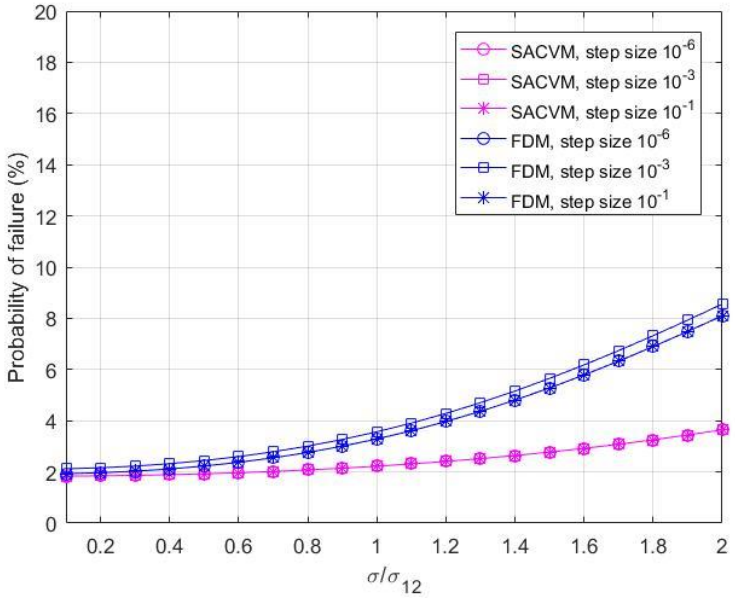

(l)

Figure 4.3 For Case 2, Probability of failure Vs Standard Deviation of random variables(normalized with their original values) (a) PWB (b) Copper Pads (c) Solder Mask (d) Polyimide Tape (e) Solder Balls (f) BT Substrate (g) Die Attach (h) Silicon Die (i) Epoxy Mold Compound (j) Heat Source (k) Heat Transfer Coefficient (l) Ambient Temperature

In this case probability of failure is most sensitive to the uncertainties present in heat transfer coefficient followed by PWB and T_{amb}. Randomness in BT substrate and Epoxy mold compound also have a little effect on the probability of failure. The rest of the random variables, on the other hand, has no effect on the probability of failure for the selected range of standard deviation whatsoever. From the plots, it is clear that SACVM performs better than FDM. SACVM calculated accurate values of sensitivities for every step size. FDM, on the other hand, produced an error in sensitivity calculations. Table 4.4 compares the performance of SACVM

and FDM for different step sizes in the calculation of the probability of failure. SACVM consistently calculated exact same values for every step size. However, FDM showed error compared to SACVM and also had convergence issues when step size is chosen below or equal to the value of 10^{-8}.

It also worthwhile to notice that probability of failure for Case 2 is significantly more than Case1, which implies that uncertainties in heat transfer effect significantly affects the reliability of the package.

Table 4.4 Comparison of FDM and SACVM in calculating the probability of failure (CASE2)

Step Size	**Probability of Failure**	
	SACVM	**FDM**
10^{-1}	2.2238	3.2713
10^{-3}	2.2238	3.2877
10^{-6}	2.2238	3.2877
10^{-8}	2.2238	-
10^{-10}	2.2238	-

Chapter 5 CONCLUSION AND FUTURE WORK

A numerical study was done to find the probability of failure of a BGA model with known design parameters. Failure criterion was defined by the average temperature between the die and heat spreader. Galerkin's finite element method was used to get the solution for temperature. The average temperature for the model was calculated to be 88.14℃. First order reliability method was used to calculate the probability of failure of the BGA package.

Trends of the probability of failure with respect to uncertainties in random parameters were plotted. Two cases were studied; one with uncertainties only in material conductivities and heat source; other with uncertainties in material conductivities, heat source, heat transfer coefficient and ambient temperature.

For Case 1, the probability of failure increased the most compared to other parameters when the standard deviation of the conductivity of PWB was increased. For BT substrate and epoxy mold compound, it increased a little. For every other parameter, there was almost no change in the probability of failure. This implies that in order to get a highly reliable BGA package we need a tighter tolerance in manufacturing PWB so that the randomness in its thermal conductivity could be reduced. At the same time, other materials don't need high tolerance in manufacturing which could be crucial in driving down the cost factors.

For Case 2, the probability of failure is considerably greater than case 1. It increased from 0.0015% to 2.22%, which shows that uncertainties in heat transfer

coefficient and ambient temperature have a significant effect on the reliability of the package. Results of case 2 showed that probability of failure increased the most as compared to other parameters when the standard deviation of heat transfer coefficient is increased. There is a minor increase in the probability of failure for PWB, BT substrate, epoxy mold compound, and ambient temperature. For every other parameter probability of failure does not change considerably. The results imply that we need a strong tolerance in setting the value of heat transfer coefficient, which in turns depends on the flow of the fluid and its thermal properties. Similarly, high manufacturing tolerance for PWB, BT substrate, and epoxy mold compound could help in removing the randomness in their conductivities, which in turn will improve the reliability of the package. Also, for those materials which did not impact probability of failure, low manufacturing tolerance can be chosen which will drive down the cost of the package.

Performance of SACVM and FDM in calculating sensitivities were also compared. It was observed that SACVM evaluated exact values for every step sizes and FDM showed error in calculations which could be attributed to cancellation and truncation error present in FDM. FDM is not suitable for problems involving a large number of variables with a huge range of values, as it becomes difficult to find perfect step sizes to calculate the accurate values of sensitivities. SACVM, on the other hand, does not depend on step size, which makes it perfect for such kind of problems.

Case 2 is a better representation of the probability of failure of the package because it also incorporates the uncertainties in heat transfer coefficient as well as ambient temperature. It should be noted however that the results are for the selected range of standard deviations. This study can be replicated to include a different range of standard deviations which suits the BGA manufacturers' need. Effects of other parameters like geometry, thermal contact resistance, etc. could also be studied in the future studies.

This study was based on the failure criterion defined by the limiting temperature at the interface of the die and heat spreader. Future studies could use a different failure criterion like thermal stress or a combination of different failures which could paint a clearer picture of the reliability of the package. The more rigorous future study could involve non-constant values of thermal conductivities and heat source. To get a complete picture a transient analysis could be done to evaluate the behavior of reliability with respect to time.

Chapter 6 REFERENCES

[1] Haldar, A. and Mahadevan, S., 2000. *Reliability assessment using stochastic finite element analysis*. John Wiley & Sons.

[2] Jin, W., 2008. *Semi-analytical complex variable based stochastic finite element method* (Doctoral dissertation, The University of Texas at Arlington).

[3] Dennis, B.H., Han, Z.X. and Dulikravich, G.S., 2003, January. Determination of temperatures and heat fluxes on surfaces and interfaces of multi-domain three-dimensional electronic components. In *ASME 2003 International Mechanical Engineering Congress and Exposition* (pp. 263-270). American Society of Mechanical Engineers.

[4] Stefanou, G., 2009. The stochastic finite element method: past, present, and future. *Computer Methods in Applied Mechanics and Engineering*, *198*(9-12), pp.1031-1051.

[5] Ghanem, R.G. and Spanos, P.D., 1991. Stochastic finite elements: a spectral approach.

[6] Chen, N.Z. and Soares, C.G., 2008. Spectral stochastic finite element analysis for laminated composite plates. *Computer Methods in Applied Mechanics and Engineering*, *197*(51-52), pp.4830-4839.

[7] Arregui-Mena, J.D., Margetts, L. and Mummery, P.M., 2016. Practical application of the stochastic finite element method. *Archives of Computational Methods in Engineering*, *23*(1), pp.171-190.

[8] Lim, J., Lee, B., and Lee, I., 2014. Second-order reliability method-based inverse reliability analysis using Hessian update for accurate and efficient reliability-based design optimization. *International Journal for Numerical Methods in Engineering*, *100*(10), pp.773-792.

[9] Rackwitz, R. and Flessler, B., 1978. Structural reliability under combined random load sequences. *Computers & Structures*, *9*(5), pp.489-494.

[10] Hien, T.D. and Kleiber, M., 1997. Stochastic finite element modelling in linear transient heat transfer. *Computer Methods in Applied Mechanics and Engineering*, *144*(1-2), pp.111-124.

[11] Grisham, J., Akbariyeh, A., Jin, W., Dennis, B.H. and Wang, B.P., 2018. Semi-Analytic Complex Variable Method for Computing Sensitivities in Heat Transfer Problems. *Journal of Heat Transfer*.

[12] Jin, W., Dennis, B.H. and Wang, B.P., 2010. Improved sensitivity analysis using a complex variable semi-analytical method. *Structural and Multidisciplinary Optimization*, *41*(3), pp.433-439.

[13] Reddy, J.N. and Gartling, D.K., 2010. *The finite element method in heat transfer and fluid dynamics*. CRC press.

[14] Hutton, D.V. and Wu, J., 2004. *Fundamentals of finite element analysis* (Vol. 1). New York: McGraw-hill.

[15] Patil, S., Chintamani, S., Kumar, R. and Dennis, B.H., 2016, November. Determination of Orthotropic Thermal Conductivity in Heat Generating Cylinder.

In *ASME 2016 International Mechanical Engineering Congress and Exposition* (pp. V011T15A016-V011T15A016). American Society of Mechanical Engineers.

[16] Patil, S., Chintamani, S., Grisham, J., Kumar, R. and Dennis, B.H., 2015, November. Inverse Determination of Temperature Distribution in Partially Cooled Heat Generating Cylinder. In *ASME 2015 International Mechanical Engineering Congress and Exposition* (pp. V08BT10A024-V08BT10A024). American Society of Mechanical Engineers.

[17] Fabela, O., Patil, S., Chintamani, S. and Dennis, B.H., 2017, November. Estimation of Effective Thermal Conductivity of Porous Media Utilizing Inverse Heat Transfer Analysis on Cylindrical Configuration. In *ASME 2017 International Mechanical Engineering Congress and Exposition* (pp. V008T10A089-V008T10A089). American Society of Mechanical Engineers.

[18] Hasofer, A.M. and Lind, N.C., 1974. Exact and invariant second-moment code format. *Journal of the Engineering Mechanics division*, *100*(1), pp.111-121.

[19] Yanfang, Z., Yanlin, Z. and Yimin, Z., 2011. Reliability sensitivity based on first-order reliability method. *Proceedings of the Institution of Mechanical Engineers, Part C: Journal of Mechanical Engineering Science*, *225*(9), pp.2189-2197.

[20] Parameswaran, N., Kjerengtroen, L., 1994. Determination of failure probabilities and sensitivity factors based on first order reliability

method. *American Society of Mechanical Engineers, Design Engineering Division (Publication) DE*, v 69-1, p 495-501, *20th Design Automation Conference*.

[21] Jin, W., Dennis, B.H., He, X., Wang, B.P. and Gao, Z., 2014, July. FORM Based Reliability Analysis With Accurate Sensitivity for Heat Conduction. In *ASME 2014 12th Biennial Conference on Engineering Systems Design and Analysis* (pp. V001T04A006-V001T04A006). American Society of Mechanical Engineers.

[22] Abubakar, U., Mohammed, I.A., Dan-asabe, B. and Alkali, A., 2014. Reliability based performance modelling and evaluation: A case study of heat exchanger. *Journal homepage: www. IJEE. IEEFoundation. org*, *5*(2), pp.257-268.

[23] Hirohata, K, Hisano, K, Mukai, M, Takahashi, H, Kawamura, N, Iwasaki, H, Kawakami, T, Yu, Q & Shiratori, M 2004, Multidisciplinary reliability design of electronics packaging based on the first order reliability method and structural equation modeling. in *Collection of Technical Papers - 10th AIAA/ISSMO Multidisciplinary Analysis and Optimization Conference.* vol. 6, pp. 3571-3589

Chapter 7 BIOGRAPHIC INFORMATION

Rahul received his bachelor's degree in mechanical engineering from G.B. Pant University of Agriculture and Technology, Pantnagar in 2015. He joined the University of Texas at Arlington in Fall 2016 to get his Master of Science degree in mechanical engineering. He joined CFD lab in fall 2016. While working there, he worked on Syngas Reforming project along with this research. He got interested in reduced order models and machine learning towards the end of his program. He plans to learn more about it in future.